Geophysical Journal International

Thermal expansivity, heat capacity and bulk modulus of the mantle

Lars Stixrude [ORCID] and Carolina Lithgow-Bertelloni

Department of Earth, Planetary, and Space Sciences, University of California, Los Angeles, CA, USA. E-mail: lstixrude@epss.ucla.edu

SUMMARY
We derive exact expressions for the thermal expansivity, heat capacity and bulk modulus for assemblages with arbitrarily large numbers of components and phases, including the influence of phase transformations and chemical exchange. We illustrate results in simple two-component, two-phase systems, including Mg–Fe olivine-wadsleyite and Ca–Mg clinopyroxene-orthopyroxene and for a multicomponent model of mantle composition in the form of pyrolite. For the latter we show results for the thermal expansivity and heat capacity over the entire mantle pressure–temperature regime to 40 GPa, or a depth of 1000 km. From the thermal expansivity, we derive a new expression for the phase buoyancy parameter that is valid for arbitrarily large numbers of phases and components and which is defined at every point in pressure–temperature space. Results reveal regions of the mantle where the magnitude of the phase buoyancy parameter is larger in magnitude than for those phase transitions that are most commonly included in mantle convection simulations. These regions include the wadsleyite to garnet and ferropericlase transition, which is encountered along hot isentropes (e.g. 2000 K potential temperature) in the transition zone, and the ferropericlase and stishovite to bridgmanite transition, which is encountered along cold isentropes (e.g. 1000 K potential temperature) in the shallow lower mantle. We also show the bulk modulus along a typical mantle isentrope and relate it to the Bullen inhomogeneity parameter. All results are computed with our code HeFESTo, updates and improvements to which we discuss, including the implementation of the exact expressions for the thermal expansivity, heat capacity and bulk modulus, generalization to allow for pressure dependence of non-ideal solution parameters and an improved numerical scheme for minimizing the Gibbs free energy. Finally, we present the results of a new global inversion of parameters updated to incorporate more recent results from experiment and first principles theory, as well as a new phase (nal phase), and new species: Na-majorite and the $NaAlO_2$ end-member of ferropericlase.

Key words: Composition and structure of the mantle; Equations of state; High-pressure behaviour; Phase transitions; Mantle processes.

1 INTRODUCTION

The thermodynamic properties of the mantle are central to our understanding of mantle dynamics, the interpretation of seismological observations and the interpretation of mantle-derived rocks. For example, mantle convection is driven largely by thermal buoyancy, the magnitude of which is determined by the thermal expansivity. The heat capacity governs the thermal response to changes in energy, for example due to radioactive decay. The bulk modulus is central to our understanding of seismic wave propagation and Earth structure.

The mantle is a multiphase assemblage, and as such displays thermodynamic properties that may differ in magnitude and sign from those of a single phase. In the presence of phase transitions, the thermal expansivity may reverse sign, as in the case of the bridgmanite forming reaction, stabilizing the flow against convection locally (Schubert *et al.* 1975; Christensen & Yuen 1985; Tackley *et al.* 1993). Depending on the sign of the Clapeyron slope of the phase transition, the thermal expansivity may also be locally enhanced by orders of magnitude, as in the case of the olivine to wadsleyite transition (Schubert *et al.* 1975). Phase transitions affect the heat capacity: the change in enthalpy with temperature upon crossing a phase transition includes the heat of reaction and so is greater than the heat capacity of the transforming phases (Schubert *et al.* 1975). The response of the mantle to seismic wave propagation is usually assumed to occur in the isomorphic limit, in which phase transformations and chemical exchange are not excited by the passage of the seismic wave; the bulk modulus sensed by seismology may differ by orders of magnitude from the equilibrium value of the transforming assemblage, leaving scope for bulk attenuation at finite frequency (Jackson 2007; Li & Weidner 2008; Ricard *et al.* 2009; Durand *et al.* 2012).

Early studies of the effects of phase transformations on mantle convection did not include all phase transformations, rather a discrete subset that are narrow and so appeared in linearized approximations. For example, Schubert *et al.* (1975) and many subsequent studies considered the olivine to wadsleyite to ringwoodite transitions, and the post-ringwoodite transition. While some subsequent studies included a larger set of discrete phase transformations (Nakagawa & Tackley 2004; Ichikawa *et al.* 2014; Arredondo & Billen 2017), this approach is limited because some important phase transitions may not be included in the list of those considered and because phase transformations in the mantle are not limited to those that are narrow. Indeed, phase transformations and chemical exchange occur at every pressure–temperature point in the upper 800 km of the mantle. Previous studies of the effects of phase transformations on bulk attenuation have also focused on individual phase transformations, particularly the olivine to wadsleyite transformation (Jackson 2007; Li & Weidner 2008; Ricard *et al.* 2009; Durand *et al.* 2012).

The advent of thermodynamic methods capable of producing comprehensive models of mantle phase equilibria and physical properties (Connolly 2005; Ricard *et al.* 2005; Stixrude & Lithgow-Bertelloni 2005a; Khan *et al.* 2006; Piazzoni *et al.* 2007; Stixrude & Lithgow-Bertelloni 2011) motivates a different strategy for investigating the influence of phase transformations on geophysical processes. With this capability, it is no longer necessary to explicitly treat individual phase transformations discreetly, nor to linearize their influence on thermodynamic properties. Thermodynamic properties can now be computed at every point in pressure–temperature space for compositions of arbitrarily large numbers of components, and assemblages consisting of arbitrarily large number of phases. The set of thermodynamic properties that can be computed include, in principle, all equilibrium properties of any equilibrium state of the system (Callen 1960). An exception has been the properties of interest here. We are not aware of any previous derivation of the thermal expansivity, heat capacity, or bulk modulus in transforming assemblages. Instead, previous approaches have estimated these quantities via finite difference, including our own earlier work (Stixrude & Lithgow-Bertelloni 2007).

Our goal is two-fold: (1) to derive exact expressions for the thermal expansivity, heat capacity, and bulk modulus that include the influence of phase transformations and (2) to illustrate the results over the entire pressure–temperature regime relevant to the upper 1000 km of the mantle, focusing on pyrolite as a model bulk composition. To better compare with previous studies of mantle convection, we express our results also in terms of a generalized phase buoyancy parameter, a quantity that has proved useful in understanding the role of phase transformations in mantle convection (Christensen 1995). Our results lead us to highlight two transitions that have not been widely considered in previous mantle convection studies and which may have an important influence on dynamics. We focus mainly on the upper 1000 km because this is where our knowledge of the phase equilibria and physical properties is most secure and because this is where the influence of phase transformations on thermodynamic properties are most important, although we do explore also effects of the perovskite to post-perovskite transition on the bulk modulus.

To apply our theory to mantle assemblages, we make use of our code, HeFESTo (Stixrude & Lithgow-Bertelloni 2005b, 2011). We have expanded the capabilities of HeFESTo as part of this study to include the computation of the thermal expansivity, heat capacity and bulk modulus. In the course of generalizing the code, we found that the computation of these properties provides a very sensitive test of the quality of the Gibbs free energy minimization algorithm. We have therefore undertaken a modification of the minimization algorithm, which substantially improves the quality of the solutions (Appendix A). In order to provide the best estimates of the values of thermal expansivity, heat capacity and bulk modulus of mantle assemblages, we have accounted for continuing rapid advance in experimental and theoretical petrology and mineral physics, by expanding the scope of HeFESTo via the addition of new phases and species and a new global inversion of parameter values (Appendix B).

2 THEORY

2.1 Overview and background

We derive analytical expressions for the thermal expansivity, heat capacity, and bulk modulus. We begin with thermodynamic background starting with the fundamental thermodynamic relation: the Gibbs free energy expressed as a function of pressure, temperature, and the amounts of the species. We then proceed with the derivation of the desired thermodynamic quantities, focusing initially on computing the temperature or pressure dependence of the amounts of the species. Finally, we provide a generalization of the phase buoyancy parameter.

The Gibbs free energy of a multiphase assemblage

$$\mathcal{G}(P, T, \vec{n}) = \sum_i^{\text{species}} n_i \mu_i(P, T, \vec{n}) = \sum_i^{\text{species}} n_i \left[\mathcal{G}_i(P, T) + RT \ln a_i(\vec{n}) \right], \tag{1}$$

where n_i, μ_i, $\mathcal{G}_i$ and a_i are, respectively, the amount, chemical potential, Gibbs free energy in the magnetically and cation-ordered pure form, and activity of species i. We assume that the quantity $RT\ln f_i$, where f_i is the activity coefficient of species i, is independent of temperature, but permit linear variations in this quantity with pressure, a generalization of our previous work (Stixrude & Lithgow-Bertelloni 2011) that is further discussed in Appendix A3. This assumption permits non-ideal enthalpy and volume of solution, and neglects the contribution of non-ideality to the entropy, because such contributions are small compared with uncertainties in the entropy at mantle pressure and temperature (Stixrude & Lithgow-Bertelloni 2011).

We focus our study on conditions of thermodynamic equilibrium. Equilibrium is a reasonable assumption throughout much of the Earth's mantle because of the high temperatures that are typical of this region: the time scale required to achieve equilibrium is short compared with that of most geological processes. We discuss the implications of departures from equilibrium that may occur, for example, in the colder portions of the mantle, as might be encountered in subducted slabs, and in the process of seismic wave propagation, where the time scale of deformation may be very short compared to that needed to achieve equilibrium.

Eq. (1) is a fundamental thermodynamic relation in the sense of Callen (1960): a single functional relationship that contains complete information of all equilibrium properties of all equilibrium states of the system. For example, the first derivatives of $\mathcal{G}$ yield the volume and entropy of the assemblage

$$\mathcal{V} = \left(\frac{\partial \mathcal{G}}{\partial P} \right)_{T,\vec{n}} = \sum_i n_i \left(\frac{\partial \mu_i}{\partial P} \right)_{T,\vec{n}} = \sum_i n_i \bar{\mathcal{V}}_i \tag{2}$$

$$\mathcal{S} = -\left(\frac{\partial \mathcal{G}}{\partial T} \right)_{P,\vec{n}} = -\sum_i n_i \left(\frac{\partial \mu_i}{\partial T} \right)_{P,\vec{n}} = \sum_i n_i \bar{\mathcal{S}}_i, \tag{3}$$

where the derivatives are taken at constant values of the amounts of all species n_i, and $\bar{\mathcal{V}}_i$ and $\bar{\mathcal{S}}_i$ are, respectively, the partial molar volume and entropy of species i. If $RT \ln f_i$ is independent of pressure and temperature, then $\bar{\mathcal{V}}_i = \mathcal{V}_i$ and $\bar{\mathcal{S}}_i = \mathcal{S}_i - R \ln a_i$, where $\mathcal{V}_i$ and $\mathcal{S}_i$ are, respectively, the volume and entropy of pure species i.

The thermal expansivity, heat capacity and bulk modulus are given by pressure and temperature derivatives of $\mathcal{V}$ and $\mathcal{S}$ in a closed system in equilibrium

$$\alpha = \frac{1}{\mathcal{V}} \left(\frac{\partial \mathcal{V}}{\partial T} \right)_{P,\vec{b}} \tag{4}$$

$$C_P = T \left(\frac{\partial \mathcal{S}}{\partial T} \right)_{P,\vec{b}} \tag{5}$$

$$K_T = -\mathcal{V} \left(\frac{\partial P}{\partial \mathcal{V}} \right)_{T,\vec{b}} \tag{6}$$

and the derivatives are taken at constant bulk composition and at chemical equilibrium so that $\sum_i \mu_i \mathrm{d}n_i = 0$.

Proceeding with the thermal expansivity as an example, combining eqs (2) and (4)

$$\alpha = \frac{1}{\mathcal{V}} \sum_i n_i \left(\frac{\partial \bar{\mathcal{V}}_i}{\partial T} \right)_{P,\vec{n}} + \frac{1}{\mathcal{V}} \sum_i \bar{\mathcal{V}}_i \left(\frac{\partial n_i}{\partial T} \right)_{P,\vec{b}} = \frac{1}{\mathcal{V}} \sum_i n_i \bar{\mathcal{V}}_i \alpha_i + \frac{1}{\mathcal{V}} \sum_i \bar{\mathcal{V}}_i \left(\frac{\partial n_i}{\partial T} \right)_{P,\vec{b}} = \alpha_{\mathrm{iso}} + \alpha_{\mathrm{met}}. \tag{7}$$

The thermal expansivity consists of two contributions. The first term

$$\alpha_{\mathrm{iso}} = \frac{1}{\mathcal{V}} \left(\frac{\partial \mathcal{V}}{\partial T} \right)_{P,\vec{n}} \tag{8}$$

is the isomorphic term, and differs from the total thermal expansivity (eq. 4) in that the derivative is taken at constant amounts of all species $\vec{n}$ rather than at constant bulk composition $\vec{b}$. The isomorphic term depends only on the properties of the end-member species, including their thermal expansivity α_i. The second term α_{met} is the metamorphic term and depends on how the amounts of species change with increasing temperature in equilibrium at constant bulk composition.

Similarly, the heat capacity is, combining eqs (3) and (5)

$$C_P = T \sum_i n_i \left(\frac{\partial \bar{\mathcal{S}}_i}{\partial T} \right)_{P,\vec{n}} + T \sum_i \bar{\mathcal{S}}_i \left(\frac{\partial n_i}{\partial T} \right)_{P,\vec{b}} = \sum_i n_i C_{Pi} + T \sum_i \bar{\mathcal{S}}_i \left(\frac{\partial n_i}{\partial T} \right)_{P,\vec{b}} = C_{\mathrm{iso}} + C_{\mathrm{met}}, \tag{9}$$

where the isomorphic term C_{iso} depends only on the heat capacities of the end-member species C_{Pi}. The bulk modulus is related to the compressibility k_T by, combining eqs (2) and (6)

$$\frac{1}{K_T} = k_T = -\frac{1}{V} \sum_i n_i \left(\frac{\partial \bar{\mathcal{V}}_i}{\partial P} \right)_{T,\vec{n}} - \frac{1}{V} \sum_i \bar{\mathcal{V}}_i \left(\frac{\partial n_i}{\partial P} \right)_{T,\vec{b}} = \frac{1}{V} \sum_i n_i \frac{V_i}{K_{Ti}} - \frac{1}{V} \sum_i \bar{\mathcal{V}}_i \left(\frac{\partial n_i}{\partial P} \right)_{T,\vec{b}} = k_{\mathrm{iso}} + k_{\mathrm{met}}, \tag{10}$$

where the isomorphic contribution to $k_{\mathrm{iso}} = 1/K_{\mathrm{iso}}$ depends only on the bulk moduli and volumes of the end-member species K_{Ti}, and the metamorphic term k_{met} depends on the variation of the amounts of the species with pressure.

The definition of the thermal expansivity, heat capacity and bulk modulus are often given as the isomorphic contribution alone with derivatives taken at constant $\vec{n}$, for example eq 8 for the thermal expansivity (Callen 1960). However in multiphase systems, the isomorphic term accounts for only part of the change in volume with temperature, and is equal to the thermal expansivity only in the special case that no chemical exchange occurs between coexisting phases on heating, either because no chemical exchange occurs in equilibrium (e.g. olivine+quartz) or because equilibrium cannot be established on the time scale of the experiment. The thermal expansivity, heat capacity, and bulk modulus (eqs 4–6), including contributions from phase transformations, have sometimes been referred to as effective values in the geophysics literature (Schubert *et al.* 1975; Christensen 1995; Nakagawa *et al.* 2009).

2.2 Thermal expansivity, heat capacity and bulk modulus

The thermodynamic properties (eqs 7, 9 and 10) have two contributions: an isomorphic term, which is readily computed as it depends only on the properties of the end-member species, and a metamorphic term, for which we must derive an expression for the temperature and pressure dependence of the amounts of the species n_i in equilibrium and at constant bulk composition. We begin with the temperature dependence of n_i; the derivation of the pressure dependence is similar. Throughout this derivation we assume the Einstein summation convention. We start with the thermodynamic identity

$$\left(\frac{\partial \mu_j}{\partial n_i}\right)_{P,T} \left(\frac{\partial n_i}{\partial T}\right)_P = -\left(\frac{\partial \mu_j}{\partial T}\right)_{P,\bar{n}} = \bar{\mathcal{S}}_j \tag{11}$$

or

$$H_{ji}\left(\frac{\partial n_i}{\partial T}\right)_P = -\left(\frac{\partial \mu_j}{\partial T}\right)_{P,\bar{n}}, \tag{12}$$

where

$$H_{ij} = \left(\frac{\partial \mu_i}{\partial n_j}\right)_{P,T} = \left(\frac{\partial^2 G}{\partial n_i \partial n_j}\right)_{P,T} \tag{13}$$

is the Hessian matrix, a square, symmetric $s \times s$ matrix, where s is the number of species. In Appendix A1, we derive the analytical expression of the Hessian for the asymmetric regular solution model. Eq. (12) is a linear system of equations relating known quantities: the Hessian matrix, and the partial molar entropies to the desired quantities: the temperature dependence of the n_i. However, this system of equations is ill-posed as written: it has no solution because the Hessian matrix is singular; the singularity of the Hessian matrix follows from the Gibbs–Duhem equation. We cast a well-posed problem by applying the constraint of constant bulk composition.

We seek temperature-dependent changes in the n_i that satisfy the bulk composition

$$r_{ij}n_j = b_i, \tag{14}$$

where r_{ij} is the $c \times s$ matrix of stoichiometric coefficients, and the vector b_i specifies the amounts of the c components that make up the bulk composition. We apply the constraint of constant bulk composition by introducing the matrix V_{ij}, the columns of which are the vectors that span the null space of eq. (14). The dimensions of V_{ij} are therefore $s \times l$ with $l = s - c$, and we have

$$V_{ik}^T V_{kj} = \delta_{ij} \tag{15}$$

since the columns are normalized and mutually orthogonal; δ_{ij} is the Kroenecker delta. We find the matrix V_{ij} via singular value decomposition, as in our previous work in which we used V_{ij} to apply the constraint of constant bulk composition to our minimization of the Gibbs free energy (Stixrude & Lithgow-Bertelloni 2011). In that paper we showed a simple example of the structure of the matrix V_{ij}: in the case of the two-component olivine-wadsleyite transition, V_{ij} has two columns which can be taken to represent the Mg–Fe cation exchange reaction and changes in the proportions of *ol* and *wa* phases.

Applying the constraint of constant bulk composition to eq. (12)

$$\hat{H}_{lk}V_{ki}^T\left(\frac{\partial n_i}{\partial T}\right)_{P,\vec{b}} = -V_{lj}^T\left(\frac{\partial \mu_j}{\partial T}\right)_{P,\bar{n}}, \tag{16}$$

where

$$\hat{H}_{lk} = V_{lj}^T H_{ji} V_{ik} \tag{17}$$

with dimensions $l \times l$ is the Hessian projected onto the null space of eq. (14), and we have made use of eq. (15). Multiplying both sides of eq. (16) by the inverse of $\hat{H}$ and then by V^T we have finally

$$\left(\frac{\partial n_i}{\partial T}\right)_{P,\vec{b}} = -M_{ij}\left(\frac{\partial \mu_j}{\partial T}\right)_{P,\bar{n}} \tag{18}$$

where

$$M_{ij} = V_{ik}\hat{H}_{kl}^{-1}V_{lj}^T \tag{19}$$

is an $s \times s$ matrix, which depends only on the Hessian and the vectors spanning the null space. The derivation is valid for all but univariant phase transitions for which $(\partial n_i/\partial T)_{P,\vec{b}}$ is singular.

We now derive analytical expressions for the thermodynamic quantities, dispensing with the Einstein summation convention, and writing out sums explicitly. Substituting eq. (18) into eq. (7) and using eq. (3), the thermal expansivity

$$\alpha = \alpha_{\text{iso}} + \frac{1}{\mathcal{V}}\sum_{i,j}^{\text{species}} M_{ij}\bar{\mathcal{S}}_j\bar{\mathcal{V}}_i. \tag{20}$$

The isobaric heat capacity is, combining eqs (3), (9) and (18)

$$C_P = C_{\text{iso}} + T \sum_{i,j}^{\text{species}} M_{ij} \bar{\mathcal{S}}_j \bar{\mathcal{S}}_i. \tag{21}$$

The derivation for the isothermal bulk modulus proceeds in much the same way, but this time involving the pressure derivative of the species amounts

$$\left(\frac{\partial n_i}{\partial P}\right)_{T,\bar{b}} = -\sum_j^{\text{species}} M_{ij}\left(\frac{\partial \mu_j}{\partial P}\right)_{T,\bar{n}} = -M_{ij}\bar{\mathcal{V}}_j. \tag{22}$$

We find, combining eqs (2), (10) and (22)

$$k_T = k_{\text{iso}} + \frac{1}{\mathcal{V}} \sum_{i,j}^{\text{species}} M_{ij} \bar{\mathcal{V}}_j \bar{\mathcal{V}}_i. \tag{23}$$

Other quantities are computed from those already given

$$C_V = \frac{C_P}{1 + \alpha \gamma T} \tag{24}$$

$$K_S = K_T(1 + \alpha \gamma T) \tag{25}$$

$$\gamma = \frac{\mathcal{V}\alpha K_T}{C_P - V\alpha^2 K_T T}, \tag{26}$$

where C_V is the isochoric heat capacity, K_S is the adiabatic bulk modulus, and γ is the Grüneisen parameter. We give the derivation of eq. (24) in Appendix C.

2.3 Phase buoyancy parameter

The phase buoyancy parameter has proved useful in understanding the influence of phase transformations on mantle convection. The conventional definition is (Christensen & Yuen 1985)

$$\Pi = \frac{\Delta\rho\Gamma}{\rho^2 \alpha g h}, \tag{27}$$

where Γ is the Clapeyron slope of the phase transition, $\Delta\rho$ is the density change across the phase transition, g is the gravitational acceleration and h is the height of the convecting fluid. We generalize this definition to resolve the ambiguity in the definition of Γ and $\Delta\rho$ for all but univariant phase transformations, and to permit computation of Π across pressure–temperature space.

We define Π as

$$\Pi = \frac{\alpha/\alpha_{\text{iso}} - 1}{\mathrm{d}\Psi/\mathrm{d}\pi} = \frac{\alpha_{\text{met}}/\alpha_{\text{iso}}}{\mathrm{d}\Psi/\mathrm{d}\pi}, \tag{28}$$

where $\pi = P/\rho g h$ is the reduced pressure and Ψ is the fraction of the high pressure phase assemblage, which varies from 0 to 1 across the phase transition. To compute $\mathrm{d}\Psi/\mathrm{d}\pi$, we begin with the phase proportions

$$\psi_i = \frac{\sum_j^{\text{species}} f_{ij} n_j}{\sum_k^{\text{phases}} \sum_j^{\text{species}} f_{kj} n_j}, \tag{29}$$

where f_{ij} is the number of atoms in the formula unit of species i in phase j. We have

$$\sum_i^{\text{phases}} \psi_i = 1 \tag{30}$$

and

$$\sum_i^{\text{phases}} \frac{\partial \psi_i}{\partial \pi} = 0. \tag{31}$$

The phase proportions ψ_i are atomic fractions, that is the fraction of the total number of atoms that are contained in phase i. We have previously discussed the advantages of this measure of phase proportion as opposed to, e.g. mole fractions: the ψ_i are independent of the choice of chemical formula (Xu *et al.* 2008). Then we have

$$\frac{\mathrm{d}\Psi}{\mathrm{d}\pi} = \frac{\sum_i' \mathrm{d}\psi_i/\mathrm{d}\pi}{\psi_T} \tag{32}$$

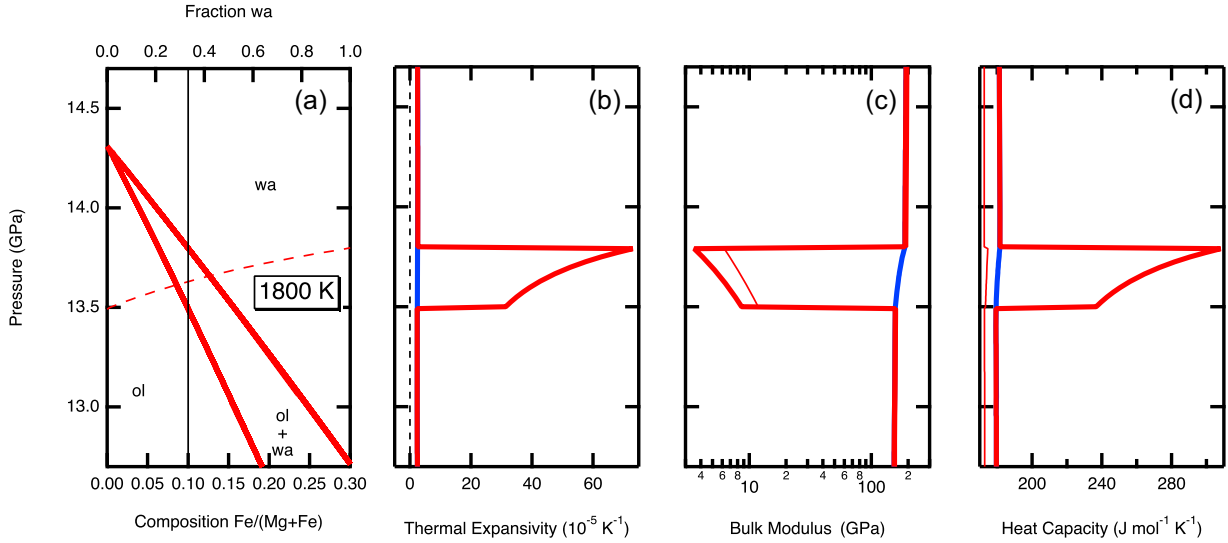**Figure 1.** (a) Mg2SiO4-Fe2SiO4 phase diagram at 1800 K (red lines), the bulk composition at which we show the physical properties of the assemblage (thin black line), and the fraction of *wa* at that bulk composition (red dashed line, top axis). The remaining panels show the total (red) and isomorphic (blue) contributions to the (b) thermal expansivity (c) bulk modulus (K_T: bold red, K_S: thin red) and (d) heat capacity (C_P: bold red, C_V: thin red). Computed with HeFESTo.

where the prime indicates that only phases i which increase in proportion with increasing pressure are included ($\mathrm{d}\psi_i/\mathrm{d}\pi > 0$) and ψ_T is the transforming phase fraction. We compute the transforming phase fraction as the mean phase fraction weighted by the rate at which the phase fractions vary with pressure

$$\psi_T = 2\frac{\sum_i \psi_i \, |\mathrm{d}\psi_i/\mathrm{d}\pi|}{\sum_i |\mathrm{d}\psi_i/\mathrm{d}\pi|}. \tag{33}$$

where we compute the $\mathrm{d}\psi_i/\mathrm{d}\pi$ by combining eqs (29) and (22) and the factor 2 guarantees that Ψ vary from 0 to 1 across the transition.

3 RESULTS

The example of the olivine to wadsleyite transition illustrates our method (Fig. 1). The metamorphic contributions to the thermal expansivity, compressibility, and heat capacity are all positive for this transition. The thermal expansivity exceeds the isomorphic contribution by more than a factor of 10 within the transformation interval, the bulk modulus is 30 times less than the isomorphic value, and the heat capacity is 30 per cent larger than the isomorphic value. The metamorphic contributions grow with increasing pressure throughout the transformation interval because the wadsleyite fraction grows at an increasing rate with increasing pressure. The non-linear dependence of the yield of the high pressure phase is a consequence of the Lever rule and has been discussed previously in the context of the seismic reflectivity of mantle phase transformations (Stixrude 1997). The metamorphic contributions to the isentropic compressibility and isochoric heat capacity are smaller than than their isothermal and isobaric counterparts, respectively.

The following approximate analysis yields additional insight into the magnitude of the metamorphic contributions

$$\alpha_{\mathrm{met}} = \frac{1}{\mathcal{V}}\sum_i \bar{\mathcal{V}}_i \left(\frac{\partial n_i}{\partial T}\right)_{P,\bar{b}} \approx \frac{\Delta \ln \mathcal{V}}{\Delta T} \approx \Gamma \frac{\Delta \ln \mathcal{V}}{\Delta P} = \Gamma \frac{\Delta \ln \rho}{\Delta P}, \tag{34}$$

where $\Delta \ln \mathcal{V}$ and $\Delta \ln \rho$ are, respectively, the fractional changes in volume and density across the transition, and ΔP is the pressure interval over which the transition occurs. The approximate equalities recognize that the value of α_{met} varies throughout the transformation interval, and that Γ has no unique definition for multi-component systems, although for sufficiently narrow transitions a sensible estimate of Γ is possible. Similarly

$$C_{\mathrm{met}} = T\sum_i \bar{\mathcal{S}}_i \left(\frac{\partial n_i}{\partial T}\right)_{P,\bar{b}} \approx \frac{T\Delta S}{\Delta T} \approx T\Gamma \frac{\Delta S}{\Delta P}, \tag{35}$$

where ΔS is the entropy of transition, and the metamorphic contribution to the compressibility

$$k_{\mathrm{met}} = -\frac{1}{\mathcal{V}}\sum_i \bar{\mathcal{V}}_i \left(\frac{\partial n_i}{\partial P}\right)_{T,\bar{b}} \approx -\frac{\Delta \ln V}{\Delta P} = \frac{\Delta \ln \rho}{\Delta P} \tag{36}$$

is always positive so that
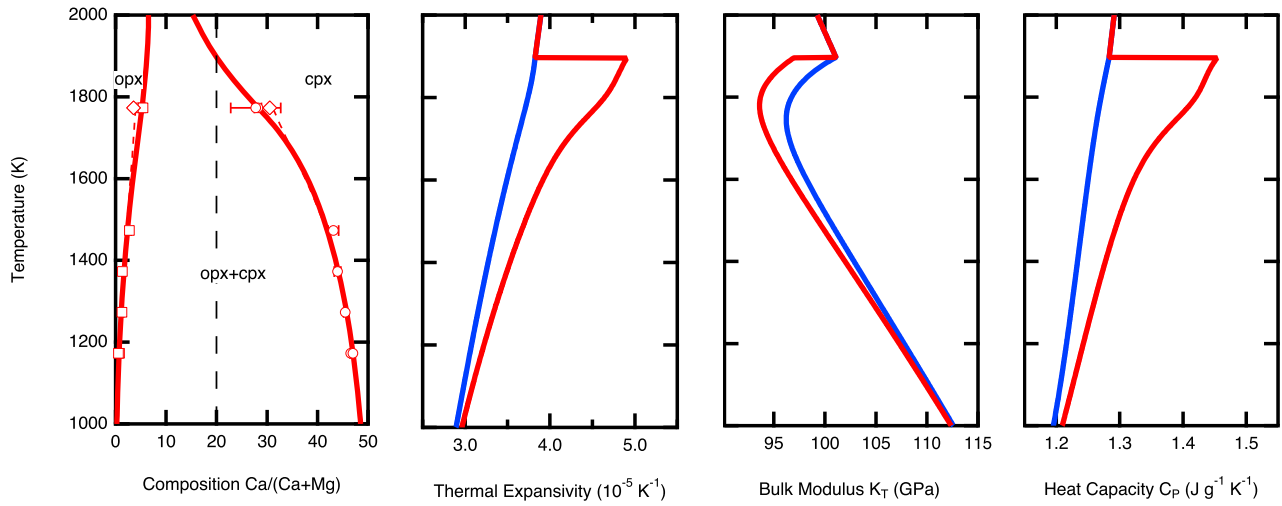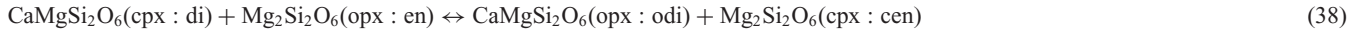
$$K_T = [k_T + k_{\mathrm{met}}]^{-1} \tag{37}$$

Figure 2. (a) $Mg_2Si_2O_6$-$CaMgSi_2O_6$ phase diagram at 3 GPa computed with HeFESTo (solid red lines) compared with experimental measurements of the compositions of the coexisting phases from Carlson & Lindsley (1988): *opx* (squares), *cpx* (circles). Also shown for comparison are the equilibria computed by HeFESTo in the CMAS system (dashed red lines) as compared with experimental observations in CMAS (Klemme & O'Neill 2000) (diamonds). The black dashed line shows the composition at which the thermal expansivity is computed. The remaining panels show the total (red) and isomorphic (blue) contributions to the (b) thermal expansivity (c) bulk modulus and (d) heat capacity at Ca/(Ca+Mg)=20 per cent.

is always less than the isomorphic bulk modulus. Taking $\Delta \ln \rho = 5.3$ per cent, $\Delta P = 0.30$ GPa, $\Gamma = 2.56$ MPa K^{-1}, $\Delta S = 5.5$ J mol^{-1} K^{-1}, eqs (34)–(37) recover values of the metamorphic contributions within the transition interval as shown in Fig. 1.

Two pyroxene equilibria on the Ca−Mg join illustrate the metamorphic contribution to thermal expansivity due to cation exchange across a very broad phase transformation (Fig. 2). The phase diagram of this system is well constrained experimentally, as are the properties of the end-member species (Domeneghetti *et al.* 1995; Tribaudino *et al.* 2001; Nestola & Tribaudino 2003). The metamorphic term grows with increasing temperature because the rate $(\partial n_i / \partial T)$ at which phase proportions change with increasing temperature increases. The positive sign of the metamorphic term is due to the positive volume of the cation exchange reaction

$$CaMgSi_2O_6(cpx : di) + Mg_2Si_2O_6(opx : en) \leftrightarrow CaMgSi_2O_6(opx : odi) + Mg_2Si_2O_6(cpx : cen) \qquad (38)$$

which proceeds to the right with increasing temperature. The positive volume of reaction can be traced to the volume of the (fictive) *odi* end-member being significantly larger than the volume of *di*, based on linear regression of the volumes of a suite of natural orthopyroxenes (Domeneghetti *et al.* 1995). Crystallographically, the positive volume of this reaction can be traced to the different configurations of the M2 site (octahedral in *opx* and an irregular eight-fold site in *cpx*): the smaller octahedral site in *opx* expands more upon replacement of Mg by Ca than does the larger eight-fold site. The abbreviations for the names of phases and species in this paragraph and throughout the remainder of the text are specified in Table A1.

Phase transformations may produce $\alpha < 0$, for phase transformations other than the widely studied bridgmanite-forming reactions. We highlight another transformation that produces $\alpha < 0$ that has not been widely appreciated: *wa=gt+fp* (Fig. 3). We show results for a model mantle composition [pyrolite, Workman & Hart (2005)] that we have examined in our previous work (Stixrude & Lithgow-Bertelloni 2011, 2012), and which consists of six oxide components: (SiO_2, MgO, FeO, CaO, Al_2O_3, Na_2O). The 18 GPa isobar (522 km depth) shows a series of three transformations with increasing temperature: *ri+st → gt*, *ri → wa*, and *wa → gt+fp*. The last causes the density to increase with increasing temperature from 2200 to 2500 K corresponding to $\alpha < 0$. Whereas the thermal expansivity may take on either sign, the bulk modulus and heat capacity are uniformly positive. We can understand the signs of the metamorphic contributions by combining eqs (34)–(36) with $\Gamma = \Delta S / \Delta V$

$$\alpha_{met} = \Gamma k_{met} \qquad (39)$$

$$C_{met} = \Gamma^2 V T k_{met}. \qquad (40)$$

Since $k_{met} > 0$, this shows that α_{met} has the sign of the Clapeyron slope while $C_{met} > 0$ regardless of the sign of Γ.

The thermal expansivity of pyrolite shows large variability over the upper 1000 km of the mantle (Fig. 4). Regions of negative thermal expansivity include the transition *wa=gt+fp* at high temperature and *fp+st=bg* at low temperature, in addition to the more widely studied bridgmanite forming reactions (*ri=bg+fp* and *ak=bg*), which occur along an average mantle isentrope. Variations in the isomorphic thermal expansivity are more subtle: α_{iso} tends to decrease with increasing pressure in the upper mantle and transition zone and then increases on crossing the bridgmanite forming reactions.

The role of phase transformations is more clearly seen in the ratio α/α_{iso} (Fig. 5, Table 1). In regions where $\alpha/\alpha_{iso} > 1$, chemical exchange enhances thermal buoyancy, for example, within the *ol = wa* transition. In regions where $\alpha/\alpha_{iso} < 0$, chemical exchange reverses the normal
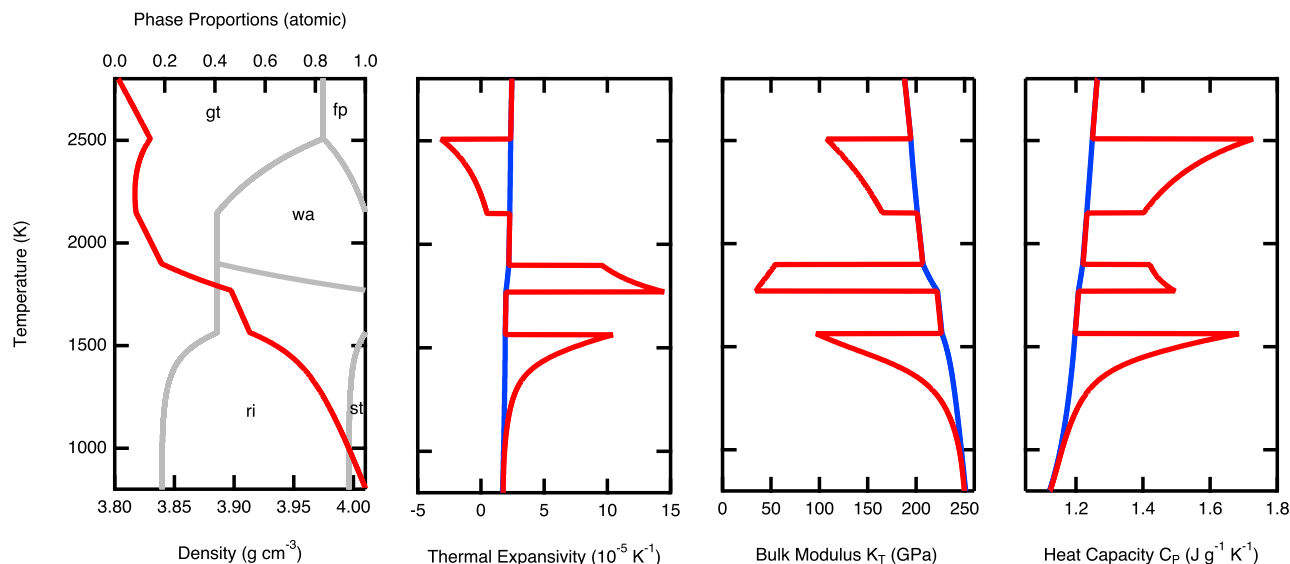
Figure 3. (a) Density (red) and phase proportions in pyrolite (grey) along the 18 GPa isobar. Total (red) and isomorphic contributions (blue) to the (b) thermal expansivity (c) bulk modulus and (d) heat capacity. Computed with HeFESTo.
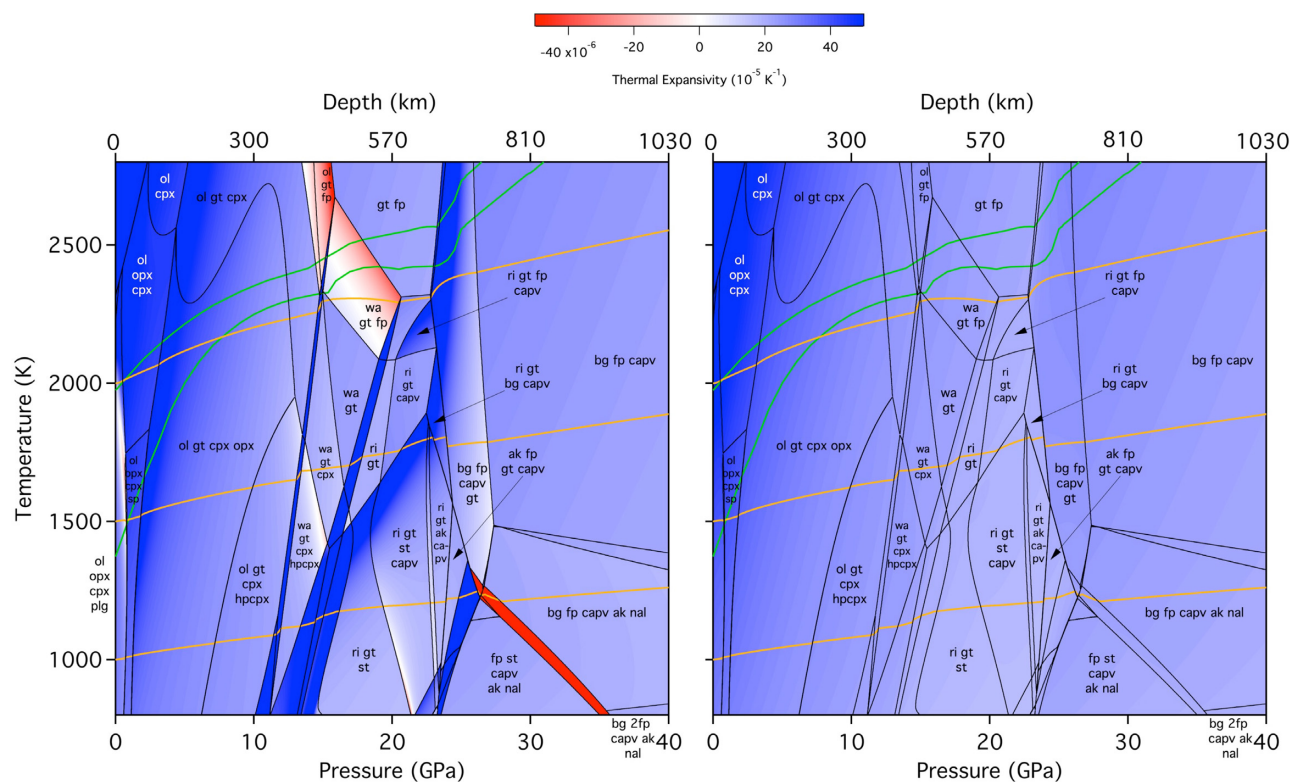

Figure 4. Left-hand panel: the thermal expansivity α of pyrolite and (right-hand panel) the isomorphic thermal expansivity α. Thin black lines represent phase transformations and text annotations indicate stability fields. Also plotted (orange lines) are self-consistently computed isentropes with potential temperatures of 1000, 1500 and 2000 K, and an estimate of the solidus and liquidus of pyrolite (green lines) from Stixrude *et al.* (2009) and based on the results of Ito *et al.* (2004), Tronnes & Frost (2002), Zhang & Herzberg (1994) and Stixrude & Karki (2005). Computed with HeFESTo on a regular pressure–temperature grid with spacings of 0.01 GPa and 1 K.

thermal buoyancy and heating increases the density, for example within the $wa + gt = wa + gt + fp$ transition, the $fp + st = bg$ transition, and the bridgmanite forming reactions. In regions where $\alpha/\alpha_{\text{iso}} \approx 1$, chemical exchange has little influence on the thermal expansivity, for example the high temperature ($T > 1500$ K) lower mantle regime in which the metamorphic contribution to the thermal expansivity, due to Mg-Fe exchange between bg and fp, is small.
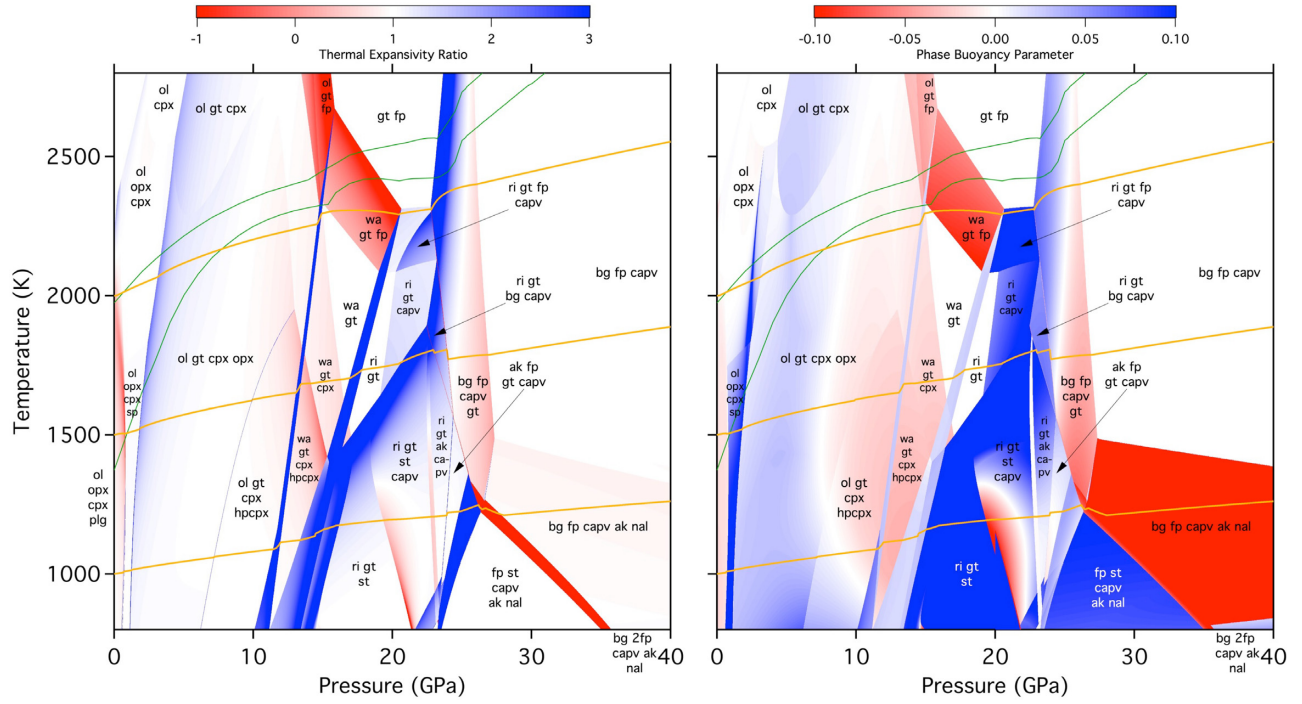
Figure 5. Left-hand panel: the ratio α/α_{iso} and (right-hand panel) the phase buoyancy parameter Π of pyrolite. The lines representing phase transitions are suppressed in these graphs so as not to obscure the properties of phase transitions, such as $ak = bg$ and $ri = bg + fp$ which occur over a very narrow range of pressure. The labels of phase stability fields, and the curves representing isentropes and the melting interval are the same as in Fig. 4. In our calculation of the phase buoyancy parameter the pressure is normalized by $\rho g h$ with $\rho = 4423$ kg m^{-3}, the mean density of the mantle in the PREM model (Dziewonski & Anderson 1981), $g = 10$ m s^{-2} and $h = 2891$ km, yielding $\rho g h = 128$ GPa. Computed with HeFESTo on a regular pressure–temperature grid with spacings of 0.01 GPa and 1 K.

Table 1. Properties of some mantle phase transformations.

Transition	T_{min} K	T_{max} K	T_a K	$P(T_{min})$ GPa	$P(T_{max})$ GPa	P_a GPa	Π	α/α_{iso}
ol=wa	1162	2677	1920	11.75	15.85	13.89	+0.0247	+13.8
ak=bg (fp)	1563	1359	1461	24.39	25.49	24.96	−0.0547	−534
ak=bg (ri)	1844	1563	1704	22.70	24.39	23.57	−0.0191	−1680
ri=bg+fp (bg)	2138	1563	1851	23.17	24.39	23.83	−0.0350	−592
ri=bg+fp (fp)	2311	2138	2225	22.77	23.17	22.97	−0.0254	−330.
wa=gt+fp	2323	2101	2306	15.37	19.12	18.08	−0.0795	−0.231
fp+st=bg	1240	800	1020	26.75	35.58	31.40	−0.104	−10.0

Notes: Transitions are reported with the low pressure assemblage first, and in parentheses, in case of multiple transitions involving the same transforming low and high pressure assemblage, a phase that appears on both sides of the transition. T_{min} and T_{max} are, respectively, the minimum and maximum temperature at which the transition occurs, and $P(T_{min})$ and $P(T_{max})$ are the corresponding pressures. The phase buoyancy parameter and the thermal expansivity ratio are evaluated at intermediate temperature T_a and the corresponding pressure $P(T_a)$. For the $wa = gt + fp$ transition, minimum and maximum pressure and temperature values correspond to the low pressure side of the phase stability region, whereas the characteristic pressure and temperature are taken to be near the middle of the phase stability region along the 2000 K isentrope.

The phase buoyancy parameter shows variations in pressure and temperature that are very similar to those of the ratio α/α_{iso} (Fig. 5, Table 1). Phase transitions for which $\alpha/\alpha_{iso} > 1$ (e.g. $ol = wa$) show a positive phase buoyancy parameter, and those with $\alpha/\alpha_{iso} < 1$ (e.g. $ri = bg + fp$) show a negative phase buoyancy parameter. Typically the magnitude of the phase buoyancy parameter increases with the magnitude of $\alpha/\alpha_{iso} - 1$, but this is not always the case. For example, within some of the broad low temperature stability fields, including $ri + gt + st$, $\alpha/\alpha_{iso} - 1$ is nearly zero, but $d\Psi/d\pi$ is also very small (the reaction $gt = ri + st$ proceeds gradually to the right with increasing pressure) so that the phase buoyancy parameter is the ratio of two small numbers, and takes on a large value ($\Pi > 0.1$). We note a final ambiguity in the definition of the phase buoyancy parameter Π suffered by the conventional definition and by our generalization. In some regions of the mantle, we find $\alpha_{met} \neq 0$ yet no pressure dependent change in phase proportions. An example is the assemblage $bg+fp+capv$. Within the scope of our model, the only chemical exchange permitted: Mg–Fe cation exchange between bg and fp, leaves the phase proportions invariant, $d\Psi/d\pi = 0$, and Π undefined. In our results below, in regions where $d\Psi/d\pi = 0$, we report $\Pi = 0$. This expedient does not fully
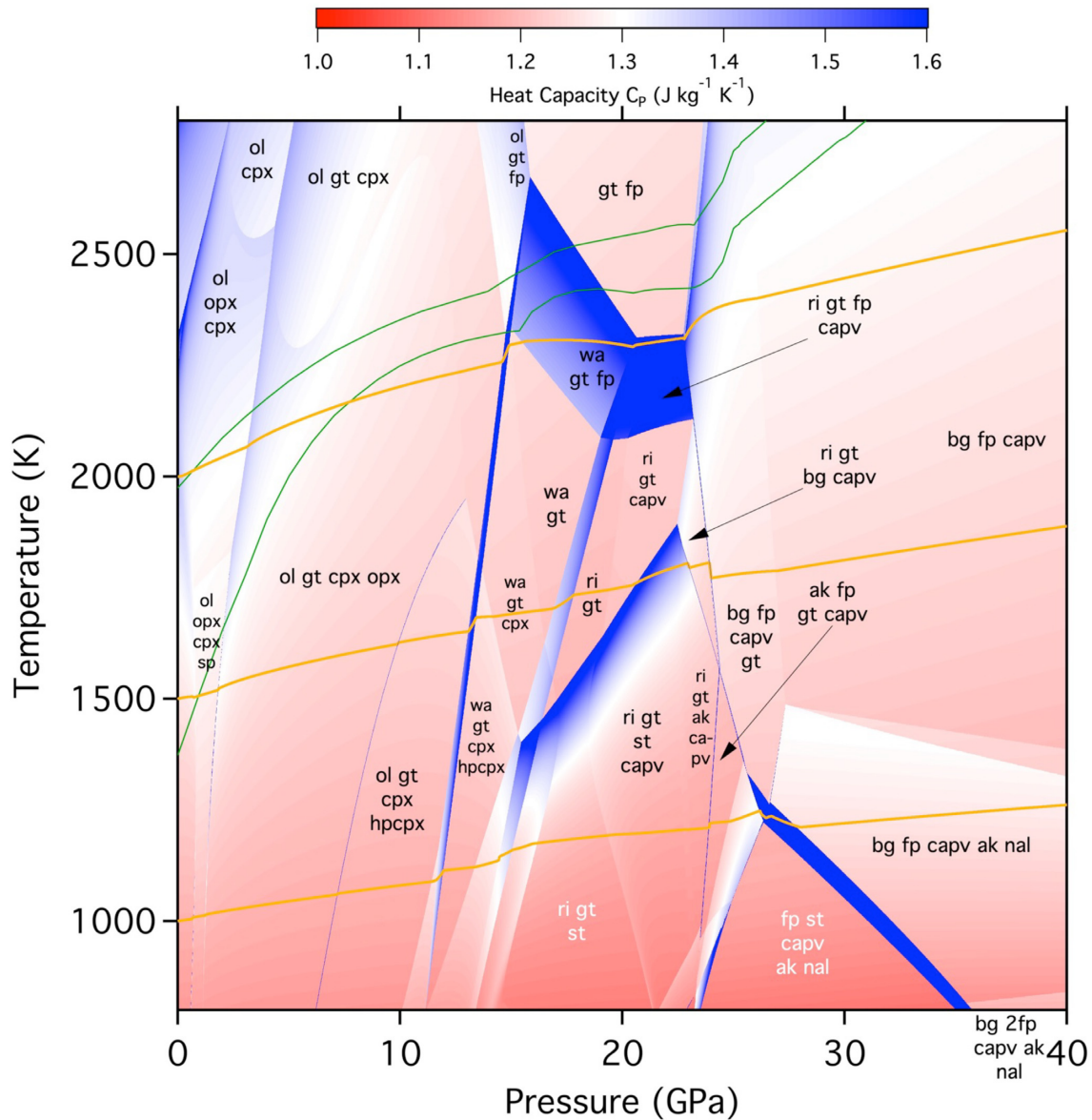
Figure 6. The heat capacity C_P. The lines representing phase transitions are suppressed so as not to obscure the properties of narrow phase transitions. The labels of phase stability fields, and the curves representing isentropes and the melting interval are the same as in Fig. 4. Computed with HeFESTo on a regular pressure–temperature grid with spacings of 0.01 GPa and 1 K.

capture the influence of chemical exchange on buoyancy, since the cation exchange reaction does contribute to the thermal expansivity, but the contribution, as we show is small (Fig. 4).

The heat capacity is everywhere larger and more variable than the isomorphic contribution (Fig. 6). For example, along the 1500 K isentrope, C_P is similar to 1.2 J g^{-1} K^{-1} and similar to C_{Piso} over most of the pressure range that we have explored, but deviates by large amounts from this value in the vicinity of phase transformations. For example, at the olivine to wadsleyite transition, the heat capacity is 1.6 J g^{-1} K^{-1}. At the $ri = bg + fp$ transition, $C_P = 15$ J g^{-1} K^{-1}, much larger than in the case of the olivine to wadsleyite transition because the bridgmanite forming reaction is much narrower.

To illustrate the influence of phase transformations on the bulk modulus, we consider the quantity (Fig. 7)

$$\eta = \frac{K_{\text{Siso}}}{K_S}. \tag{41}$$

For pyrolite along the 1500 K adiabat, the value of η deviates significantly from unity due to phase transformations. For example, the most prominent peaks, near 70, 410 and 660 km depth are due, respectively, to the $plg=sp$, $ol=wa$ and $ri=bg+fp$ transitions, while the peak near 2600 km depth is due to the $bg=ppv$ transition, which is crossed once on the 1500 K isentrope. The value of η is very nearly unity throughout most of the lower mantle (deviations of less than 10^{-5} from 721 to 2530 km depth), because Mg–Fe exchange between bg and fp has a small volume of reaction which does not depend strongly on pressure, as also found experimentally (Nakajima *et al.* 2012).
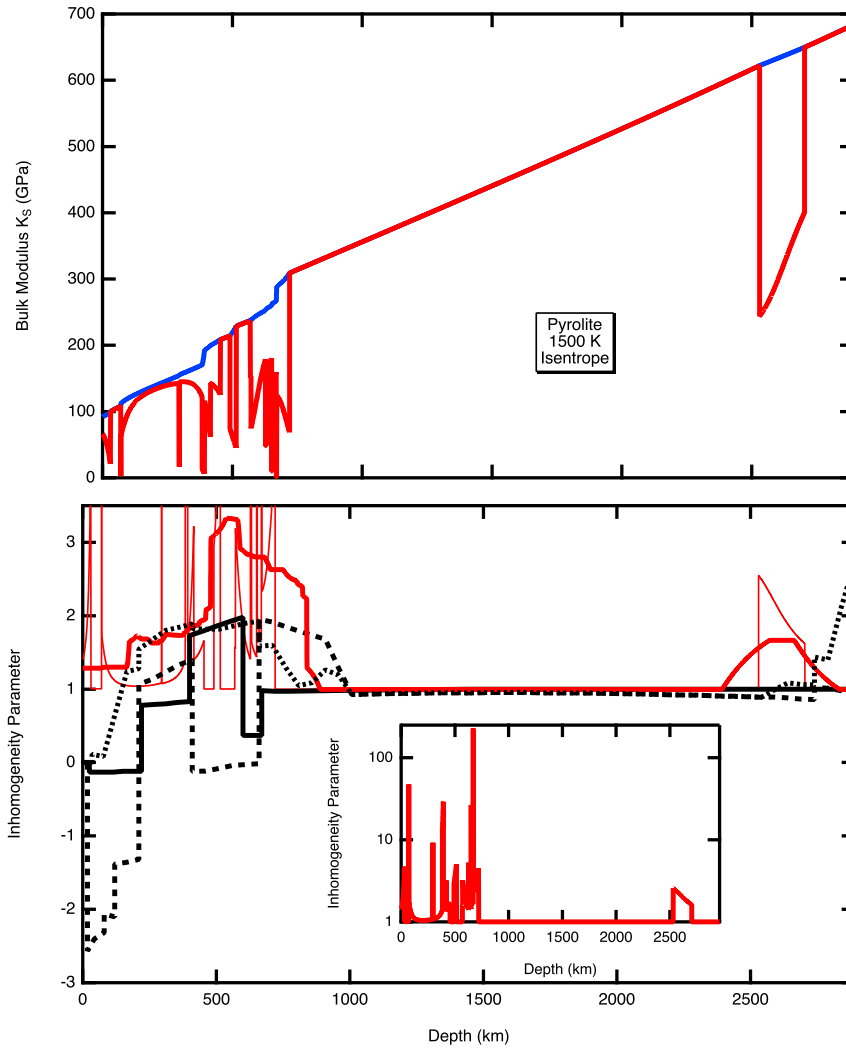
Figure 7. (top panel) The bulk modulus K_S (red) and the isomorphic contribution K_{Siso} (blue) of pyrolite along the 1500 K adiabat. (bottom) The ratio $\eta = K_{Siso}/K_S$ of pyrolite along the 1500 K adiabat (thin red line), and η smoothed with a 200 km box filter (bold red line) compared with the value of η_B from seismic models PREM (black solid line, Dziewonski & Anderson 1981), AK135f (black longer dashed line) (Montagner & Kennett 1996) and EK137 Kennett (2020) (black shorter dashed line). (bottom inset) η of pyrolite along the 1500 K adiabat on a logarithmic scale. All red and blue curves computed with HeFESTo.

4 DISCUSSION

Along a typical isentrope, our results show values of the phase buoyancy parameter for the most widely studied transitions: *ol=wa* and the *bg*-forming reactions that are similar to values of Π that have been explored in previous mantle convection studies (Tackley *et al.* 1994, Fig. 5, Table 1). Our values are somewhat smaller than those that have typically been assumed because of improved knowledge of the equations of state and Clapeyron slopes of the transforming phases that are now incorporated in HeFESTo (Appendix B).

Our results also show that the phase buoyancy along hotter and colder isentropes differs significantly from that along the average mantle isentrope (Fig. 5, Table 1). For example, along the 2000 K isentrope, which may be representative of hot mantle plumes, or the early Earth, the *wa = gt + fp* transition may significantly impede flow: the phase buoyancy parameter of the *wa = gt + fp* transition is more negative than that of the usual bridgmanite forming reactions (*ri = bg + fp* and *ak = bg*). The *wa = gt + fp* transformation can be written in terms of the magnesian end-members

$$Mg_2SiO_4(wa) = MgSiO_3(gt) + MgO(fp). \tag{42}$$

This transition occurs at supersolidus conditions in the $MgO-SiO_2$ system and the stability field of the right-hand side expands to lower temperature, subsolidus conditions with the addition of Al and Ca to the bulk composition, components which dissolve in the garnet phase, but not in the wadsleyite phase (Akaogi & Akimoto 1979). Ferropericlase is most commonly thought of as a lower mantle phase. However, several experimental phase equilibrium studies have found *gt* and *fp* coexisting within our predicted *gt + fp* stability field for bulk silicate Earth-like compositions (Zhang & Herzberg 1994; Gasparik 2000; Tronnes & Frost 2002; Hirose 2002; Frost 2003a; Ishii *et al.* 2018), and ferropericlase has been found in diamond inclusions from the transition zone (Brey *et al.* 2004). A previous mantle convection study

considered the $wa = gt + fp$ transformation (Ichikawa *et al.* 2014), finding that it tends to impede flow, although using a phase diagram that does not agree well with the experimental evidence. The influence of phase buoyancy may be greater along hotter geotherms for the same value of Π because the viscosity is smaller and the typical length scale of flow is smaller. A number of mantle convection studies have found that the influence of phase buoyancy grows with increasing Rayleigh number or decreasing length scale of the flow (Christensen & Yuen 1985; Tackley 1995).

Along the 1000 K isentrope, bridgmanite forms via the reaction $fp + st = bg$, which has a much more negative phase buoyancy parameter than the usual bridgmanite forming reactions ($ri = bg + fp$ and $ak = bg$) (Fig. 5, Table 1). The transition occurs at depths considerably deeper than 670 km: 27 GPa or 740 km along the 1000 K isentrope. This transition may therefore impede the descent of cold subducting slabs at 740 km depth. Kinetics may play an important role at such low temperatures in the mantle. The transition may be kinetically hindered in downgoing slabs and may occur at depths even greater than 740 km. The $fp + st$ stability field that we predict in peridotitic bulk compositions, as well as in simple end-member compositions such as MgSiO$_3$ and Mg$_2$SiO$_4$ (Stixrude & Lithgow-Bertelloni 2011), has not been observed experimentally, yet it does not violate experimental observations.

Understanding the effect of phase transformations on thermal expansivity is not only important for the mantle, but for practical applications as well. Considerable effort is devoted to finding materials exhibiting large negative thermal expansion, with those that show $\alpha < -10 \times 10^{-5}$ K^{-1}, classified as 'giant' or 'colossal' negative thermal expansivity materials (Takenaka 2012; Takenaka *et al.* 2017). Much of the attention in this field is focused on systems that undergo phase transformations (Azuma *et al.* 2011; Nabetani *et al.* 2015). Indeed, the mantle exceeds the colossal negative thermal expansivity threshold at many pressures and temperatures in the vicinity of phase transformations (Fig. 4, Table 1). Negative thermal expansivity occurs in some pure phases, the most famous example being water, but the magnitude is much smaller ($<2 \times 10^{-5}$ K^{-1}). Examples of pure phases that exhibit negative thermal expansivity include several minerals, such as ice (Fortes 2018), cordierite (Milberg & Blair 1977) and β-eucryptite (Gillery & Bush 1959). The origin of negative thermal expansivity in these crystalline materials, which tends to be restricted to low temperatures, is well understood and originates in bond-bending modes that are disproportionately populated at low temperature (Barron 1957).

Before discussing the comparison of η (eq. 41) to the Bullen inhomogeneity parameter (Bullen 1975), we review the relationship between these two quantities, starting with

$$\eta = \frac{K_{\text{Siso}}}{K_S} = \left(\frac{\partial P}{\partial \rho}\right)_{S,\vec{n}} \bigg/ \left(\frac{\partial P}{\partial \rho}\right)_{S,\vec{b}} = \frac{K_{\text{Siso}}}{\rho} \frac{1}{\rho g} \left(\frac{\partial \rho}{\partial z}\right)_{S,\vec{b}}. \tag{43}$$

The denominator has also been called the equilibrium or zero frequency bulk modulus ((Brown & Shankland 1981; Heinz & Jeanloz 1983; Li & Weidner 2008; Ricard *et al.* 2009), and is the bulk modulus that governs Earth structure, a relationship that we make explicit in the last relation of eq. (43) by assuming that the source of pressure is hydrostatic. The numerator is the bulk modulus probed by high frequency seismic waves and has also been referred to as the frozen or high frequency bulk modulus as it expresses the response to pressure variations that occur on time scales much shorter than those of chemical exchange (Jackson 2007; Ricard *et al.* 2009). If we generalize the derivative of density to permit variations in entropy and bulk composition with depth, and substitute $\phi = K_S/\rho = \phi = V_P^2 - 4/3 V_S^2$ into eq. (43), where V_P and V_S are, respectively, the seismologically observed values of the longitudinal and shear wave velocity, we have the Bullen inhomogeneity parameter

$$\eta_B = \frac{\phi}{\rho g} \frac{\partial \rho}{\partial z}. \tag{44}$$

In adiabatic, chemically homogeneous regions, we expect $\eta = \eta_B$, whereas in regions containing no phase transformations, we have in addition $\eta = 1$. In the presence of phase transformations, the ratio η must be greater than or equal to unity because any chemical exchange or phase transition that occurs in response to an increase in pressure increases the density at least as much as would occur in the frozen limit.

We compare our value of η to values of η_B derived from seismological models ek137 (Kennett 2020), ak135f (Kennett *et al.* 1995) and PREM (Dziewonski & Anderson 1981) in Fig. (7). Throughout most of the lower mantle, η and η_B are similar to unity. This agreement does not necessarily demonstrate that the lower mantle is close to adiabatic and homogeneous, because the density gradient, and therefore η_B is not well constrained by seismic observations (Masters 1979). Limited depth resolution means that we must also be cautious in drawing conclusions regarding the presence or absence of the $bg = ppv$ feature in η_B near 2600 km depth. There may be small differences between η and η_B, even in adiabatic, chemically homogeneous regions (quite apart from the limitation imposed by the finite spatial resolution of Earth models). The isomorphic bulk modulus K_{Siso} is derived in the limit of uniform stress among coexisting grains, known as the Reuss limit (Watt *et al.* 1976). However, the passage of a seismic wave may excite stress heterogeneity among coexisting grains and as a result sense a bulk modulus greater than the Reuss limit. Because of this effect, η_B may exceed η (Heinz & Jeanloz 1983). We must also consider the finite frequency of seismic waves: low frequency waves may have periods comparable to the time scale of chemical exchange. In this case the value of K_S sensed by the seismic probe is less than the frozen limit and $\eta_B < \eta$ (Jackson 2007; Li & Weidner 2008; Ricard *et al.* 2009; Durand *et al.* 2012). These two source of deviations of η_B from η are of interest because they are associated with bulk attenuation: a property of the mantle, the source of which is still uncertain, but which may lend valuable insight into the nature of phase transformations at depth (Durand *et al.* 2012).

Because of the trade-off between resolution and precision in the seismological models (Masters & Gubbins 2003), we have attempted to provide a more direct comparison between η and η_B by computing a smoothed version of η (Fig. 7). Our smoothed version of η shows values

greater than unity over the upper 800 km of the mantle, reflecting the influence of phase transformations in this region. Values of $\eta_B > 1$ also appear in the transition zone in the PREM model and in ek137, and in many earlier seismological models (Masters 1979). However, in the ak135 model, η_B is less than unity in the transition zone, and is even slightly less than zero near 400 km depth, emphasizing that caution is needed in interpreting η_B. In the uppermost mantle, all seismological models show $\eta_B < 1$. This feature can be explained by the upper thermal boundary layer: because temperature increases rapidly with increasing depth in this non-isentropic layer, thermal expansion counteracts and can even overcome the effect of pressure on the density, causing the density to decrease with increasing depth (Stixrude 2007).

As we have shown, it is now possible rigorously to compute in thermodynamic equilibrium, the thermal expansivity, heat capacity, and bulk modulus of the mantle, including the influence of phase transformations. An active area of research that lies well beyond the scope of this paper is the practical and robust implementation of the effect of phase transformations in geophysical fluid dynamical codes, whether focused on mantle convection, post-glacial rebound, or seismic wave attenuation. One way to appreciate the challenges is to consider the value of the thermal expansivity at the nodes of a finite spatial grid. As typical finite element grids are much coarser than the width of many phase transitions, the region in which α_{met} is large in magnitude may be entirely missed. Some approaches to this problem include computing the thermal expansivity and heat capacity by finite difference (Nakagawa *et al.* 2009), and reformulating the governing equations in terms of independent variables other than pressure and temperature (Voller & Prakash 1987; Connolly 2009). Moreover, while many computational schemes neglect the time derivative of the density in the mass conservation equation, this may not be justified: because the spatial gradient of the density may be large in the vicinity of phase transformations, flow through the phase transition entails time variations of the density that may not be negligible (Gassmoller *et al.* 2020).

5 CONCLUSIONS

We have derived expressions for the thermal expansivity, bulk modulus, and heat capacity in assemblages with an arbitrary number of phases and components, and including the influence of phase transformations. This result will be important for furthering our understanding of the influence of phase transformations on geophysical processes, and in other fields as well, including materials science. Computations of these properties for a model mantle composition show potentially important effects of phase transformations on mantle dynamics beyond those transitions usually considered. Along hot isentropes, the wadsleyite to garnet and ferropericlase transition may impede the ascent of plumes or affect dynamical layering in the early Earth. Along cold isentropes, the transformation of oxides to bridgmanite may impede the descent of slabs. It will be important to investigate the possible influence of these transformations on mantle convection, including in simulations that are able to account for the much reduced viscosity along hot isentropes, and the possible influence of kinetics along cold isentropes. The ability to compute the bulk modulus analytically may facilitate the consideration of the effects of phase transformations other than the olivine to wadsleyite transition on bulk attenuation.

DATA AVAILABILITY

The data underlying this article, including parameter values at full precision are available on GitHub at https://github.com/stixrude/HeFESTo_Parameters_010121. The code HeFESTo is available on GitHub at https://github.com/stixrude/HeFESToRepository.

REFERENCES

Ackerman, R.J. & Sorrell, C.A., 1974. Thermal-expansion and high-low transformation in quartz. 1. High-temperature X-ray studies, *J. Appl. Crystallogr.,* **7**(5), 461–467.

Adams, J.J., Agosta, D.S., Leisure, R.G. & Ledbetter, H., 2006. Elastic constants of monocrystal iron from 3 to 500 K, *J. Appl. Phys.,* **100**(11),.

Akaogi, M. & Akimoto, S., 1979. High-pressure phase-equilibria in a garnet lherzolite, with special reference to Mg^{2+}-Fe^{2+} partitioning among constituent minerals, *Phys. Earth planet. Inter.,* **19**(1), 31–51.

Akaogi, M., Hamada, Y., Suzuki, T., Kobayashi, M. & Okada, M., 1999. High pressure transitions in the system $MgAl_2O_4$-$CaAl_2O_4$: a new hexagonal aluminous phase with implication for the lower mantle, *Phys. Earth planet. Inter.,* **115**(1), 67–77.

Akaogi, M., Tanaka, A., Kobayashi, M., Fukushima, N. & Suzuki, T., 2002. High-pressure transformations in $NaAlSiO_4$ and thermodynamic properties of jadeite, nepheline, and calcium ferrite-type phase, *Phys. Earth planet. Inter.,* **130**(1–2), 49–58.

Akaogi, M., Yano, M., Tejima, Y., Iijima, M. & Kojitani, H., 2004. High-pressure transitions of diopside and wollastonite: phase equilibria and thermochemistry of $CaMgSi_2O_6$, $CaSiO_3$ and $CaSi_2O_5$-$CaTiSiO_5$ system, *Phys. Earth planet. Inter.,* **143-44**, 145–156.

Akimoto, S. & Syono, Y., 1970. High-pressure decomposition of the system $FeSiO_3$-$MgSiO_3$, *Phys. Earth planet. Inter.,* **3,** 186–188.

Anderson, O.L. & Isaak, D.G., 1995. Elastic constants of mantle minerals at high temperature, in *Mineral Physics and Crystallography: A Handbook of Physical Constants,* pp. 64–97, ed. Ahrens, T.J., American Geophysical Union.

Andrault, D., Fiquet, G. & Hanfland, M., 1998. Pressure-induced landau-type transition in stishovite, *Science,* **282,** 720–723.

Angel, R.J., Hazen, R.M., McCormick, T.C., Prewitt, C.T. & Smyth, J.R., 1988. Comparative compressibility of end-member feldspars, *Phys. Chem. Miner.,* **15**(4), 313–318.

Anovitz, L.M., Essene, E.J., Metz, G.W., Bohlen, S.R., Westrum, E.F. & Hemingway, B.S., 1993. Heat-capacity and phase-equilibria of almandine, Fe$_3$Al$_2$Si$_3$O$_{12}$, *Geochim. Cosmochim. Acta,* **57**(17), 4191–4204.

Antonangeli, D. & Ohtani, E., 2015. Sound velocity of hcp-Fe at high pressure: experimental constraints, extrapolations and comparison with seismic models, *Prog. Earth planet. Sci.,* **2,** 3,.

Aronson, M.C., Stixrude, L., Davis, M.K., Gannon, W. & Ahilan, K., 2007. Magnetic excitations and heat capacity of fayalite, Fe$_2$SiO$_4$, *Am. Mineral.,* **92**(4), 481–490.

Arredondo, K.M. & Billen, M.I., 2017. Coupled effects of phase transitions and rheology in 2-D dynamical models of subduction, *J. geophys. Res.,* **122**(7), 5813–5830.

Azuma, M., Chen, W.T., Seki, H. *et al.,* 2011. Colossal negative thermal expansion in BiNiO$_3$ induced by intermetallic charge transfer, *Nat. Commun.,* **2,** 5, doi:10.1038/ncomms1361.

Barron, T. H.K., 1957. Gruneisen parameters for the equation of state of solids, *Ann. Phys.,* **1**(1), 77–90.

Basinski, Z.S., Humerothery, W. & Sutton, A.L., 1955. The lattice expansion of iron, *Proc. R. Soc. Lond., A,* **229**(1179), 459–467.

Bass, J.D., 1995. Elasticity of minerals, glasses, and melts, in *Mineral Physics and Crystallography: A Handbook of Physical Constants,* pp. 45–63, ed. Ahrens, T.J., American Geophysical Union.

Benisek, A., Etzel, K. & Cemic, L., 2007. Thermodynamic mixing behavior of synthetic Ca-Tschermak-diopside pyroxene solid solutions: II. Heat of mixing and activity-composition relationships, *Phys. Chem. Miner.,* **34**(10), 747–755.

Bindi, L., Dymshits, A.M., Bobrov, A.V., Litasov, K.D., Shatskiy, A.F., Ohtani, E. & Litvin, Y.A., 2011. Crystal chemistry of sodium in the Earth's interior: the structure of Na$_2$MgSi$_5$O$_{12}$ synthesized at 17.5 GPa and 1700°C, *Am. Mineral.,* **96**(2–3), 447–450.

Bohlen, S.R. & Boettcher, A.L., 1982. The quartz-reversible-coesite transformation—a precise determination and the effects of other components, *J. geophys. Res.,* **87**(NB8), 7073–7078.

Bohlen, S.R., Essene, E.J. & Boettcher, A.L., 1980. Reinvestigation and application of olivine-quartz-orthopyroxene barometry, *Earth planet. Sci. Lett.,* **47**(1), 1–10.

Bosenick, A. & Geiger, C.A., 1997. Powder X-ray diffraction study of synthetic pyrope-grossular garnets between 20 and 295 K, *J. geophys. Res.,* **102**(B10), 22 649–22 657.

Bouhifd, M.A., Andrault, D., Fiquet, G. & Richet, P., 1996. Thermal expansion of forsterite up to the melting point, *Geophys. Res. Lett.,* **23**(10), 1143–1146.

Bourova, E., Richet, P. & Petitet, J.P., 2006. Coesite (SiO$_2$) as an extreme case of superheated crystal: an X-ray diffraction study up to 1776 K, *Chemical Geology,* **229**(1–3), 57–63.

Boyd, F.R. & England, J.L., 1963. Effect of pressure on melting of diopside, CaMgSi$_2$O$_6$, and albite, NaAlSi$_3$O$_8$, in range up to 50 kilobars, *J. geophys. Res.,* **68**(1), 311–323.

Boyd, F.R., England, J.L. & Davis, B. T.C., 1964. Effects of pressure on melting + polymorphism of enstatite MgSiO$_3$, *J. geophys. Res.,* **69**(10), 2101–2106.

Brey, G.P., Bulatov, V., Girnis, A., Harris, J.W. & Stachel, T., 2004. Ferropericlase—a lower mantle phase in the upper mantle, *Lithos,* **77**(1–4), 655–663.

Brown, J.M. & Shankland, T.J., 1981. Thermodynamic parameters in the earth as determined from seismic profiles, *Geophys. J. R. astr. Soc.,* **66**(3), 579–596.

Brown, J.M., Abramson, E.H. & Angel, R.J., 2006. Triclinic elastic constants for low albite, *Phys. Chem. Miner.,* **33**(4), 256–265.

Bullen, K.E., 1975. *The Earth's Density,* Chapman and Hall.

Bykova, E., Dubrovinsky, L. *et al.,* 2016. Structural complexity of simple Fe$_2$O$_3$ at high pressures and temperatures, *Nat. Commun.,* **7,** 10661, doi:10.1038/ncomms10661.

Callen, H.B., 1960. *Thermodynamics,* John Wiley and Sons.

Canil, D., 1994. Stability of clinopyroxene at pressure-temperature conditions of the transition region, *Phys. Earth planet. Inter.,* **86**(1–3), 25–34.

Caracas, R. & Cohen, R.E., 2005. Prediction of a new phase transition in Al$_2$O$_3$ at high pressures, *Geophys. Res. Lett.,* **32**(6), L06303.

Carlson, W.D. & Lindsley, D.H., 1988. Thermochemistry of pyroxenes on the join Mg$_2$Si$_2$O$_6$-CaMgSi$_2$O$_6$, *Am. Mineral.,* **73**(3–4), 242–252.

Chen, T., Gwanmesia, G.D., Wang, X.B., Zou, Y.T., Liebermann, R.C., Michaut, C. & Li, B.S., 2015. Anomalous elastic properties of coesite at high pressure and implications for the upper mantle X-discontinuity, *Earth planet. Sci. Lett.,* **412,** 42–51.

Christensen, U., 1995. Effects of phase transitions on mantle convection, *Ann. Rev. Earth planet. Sci.,* **23,** 65–87.

Christensen, U.R. & Yuen, D.A., 1985. Layered convection induced by phase transitions, *J. geophys. Res.,* **90,** 10 291–10 300.

Cohen, R.E., 1986. Thermodynamic solution properties of aluminous clinopyroxenes: non-linear least squares refinements, *Geochim. Cosmochim. Acta,* **50,** 563–575.

Comodi, P., Zanazzi, P.F., Poli, S. & Schmidt, M.W., 1997. High-pressure behavior of kyanite: compressibility and structural deformations, *Am. Mineral.,* **82**(5–6), 452–459.

Connolly, J.A.D., 2005. Computation of phase equilibria by linear programming: a tool for geodynamic modeling and its application to subduction zone decarbonation, *Earth planet. Sci. Lett.,* **236**(1–2), 524–541.

Connolly, J.A.D., 2009. The geodynamic equation of state: what and how, *Geochem. Geophys. Geosyst.,* **10**(10), doi:10.1029/2009GC002540.

Dai, L.D., Kudo, Y., Hirose, K., Murakami, M., Asahara, Y., Ozawa, H., Ohishi, Y. & Hirao, N., 2013. Sound velocities of Na$_{0.4}$Mg$_{0.6}$Al$_{1.6}$Si$_{0.4}$O$_4$ NAL and CF phases to 73 GPa determined by brillouin scattering method, *Phys. Chem. Miner.,* **40**(3), 195–201.

Dewaele, A. & Torrent, M., 2013. Equation of state of α-Al$_2$O$_3$, *Phys. Rev. B,* **88,** doi:10.1103/PhysRevB.88.064107.

Dewaele, A., Loubeyre, P., Occelli, F., Mezouar, M., Dorogokupets, P.I. & Torrent, M., 2006. Quasihydrostatic equation of state of iron above 2 mbar, *Phys. Rev. Lett.,* **97,**.

Domeneghetti, M.C., Molin, G.M. & Tazzoli, V., 1995. A crystal-chemical model for PBCA ortho-pyroxene, *Am. Mineral.,* **80**(3–4), 253–267.

Dorfman, S.M. & Duffy, T.S., 2014. Effect of Fe-enrichment on seismic properties of perovskite and post-perovskite in the deep lower mantle, *Geophys. J. Int.,* **197**(2), 910–919.

Dorfman, S.M., Prakapenka, V.B., Meng, Y. & Duffy, T.S., 2012. Intercomparison of pressure standards (Au, Pt, Mo, MgO, NaCl and Ne) to 2.5 mbar, *J. geophys. Res.,* **117,** B08210.

Dorfman, S.M., Meng, Y., Prakapenka, V.B. & Duffy, T.S., 2013. Effects of Fe-enrichment on the equation of state and stability of (Mg,Fe)SiO$_3$ perovskite, *Earth planet. Sci. Lett.,* **361,** 249–257.

Dorogokupets, P.I. & Dewaele, A., 2007. Equations of state of MgO, Au, Pt, NaCl-B$_1$, and NaCl-B$_2$: internally consistent high-temperature pressure scales, *High Press. Res.,* **27**(4), 431–446.

Downs, R.T. & Palmer, D.C., 1994. The pressure behavior of a-cristobalite, *Am. Mineral.,* **79,** 9–14.

Duan, W.H., Karki, B.B. & Wentzcovitch, R.M., 1999. High-pressure elasticity of alumina studied by first principles, *Am. Mineral.,* **84**(11–12), 1961–1966.

Dubrovinsky, L.S., Dubrovinskaia, N.A., Prokopenko, V.B. & Bihan, T.L., 2002. Equation of state and crystal structure of NaAlSiO$_4$ with calcium-ferrite type structure in the conditions of the lower mantle, *High Press. Res.,* **22**(2), 495–499.

Durand, S., Chambat, F., Matas, J. & Ricard, Y., 2012. Constraining the kinetics of mantle phase changes with seismic data, *Geophys. J. Int.,* **189**(3), 1557–1564.

Dymshits, A.M., Bobrov, A.V., Bindi, L., Litvin, Y.A., Litasov, K.D., Shatskiy, A.F. & Ohtani, E., 2013. Na-bearing majoritic garnet in the Na$_2$MgSi$_5$O$_{12}$-Mg$_3$Al$_2$Si$_3$O$_{12}$ join at 11-20 GPa: phase relations, structural peculiarities and solid solutions, *Geochim. Cosmochim. Acta,* **105,** 1–13.

Dymshits, A.M., Litasov, K.D., Shatskiy, A., Sharygin, I.S., Ohtani, E., Suzuki, A., Pokhilenko, N.P. & Funakoshi, K., 2014. P-V-T equation of state of Na-majorite to 21 GPa and 1673 K, *Phys. Earth planet. Inter.,* **227,** 68–75.

Dziewonski, A.M. & Anderson, D.L., 1981. Preliminary reference earth model, *Phys. Earth planet. Inter.,* **25,** 297–356.

Etzel, K., Benisek, A., Dachs, E. & Cemic, L., 2007. Thermodynamic mixing behavior of synthetic Ca-Tschermak-diopside pyroxene solid solutions: I. Volume and heat capacity of mixing, *Phys. Chem. Miner.,* **34**(10), 733–746.

Fei, Y., 1995. Thermal expansion, in *Mineral Physics and Crystallography: A Handbook of Physical Constants,* pp. 29–44, ed. Ahrens, T.J., American Geophysical Union.

Fei, Y., Orman, J.V. *et al.,* 2004. Experimentally determined postspinel transformation boundary in Mg_2SiO_4 using MgO as an internal pressure standard and its geophysical implications, *J. geophys. Res.,* **109**(B2),.

Fei, Y.W., Mao, H.K., Shu, J.F., Parthasarathy, G., Bassett, W.A. & Ko, J.D., 1992. Simultaneous high-p, high-t X-ray-diffraction study of beta-$(Mg,Fe)_2SiO_4$ to 26-GPa and 900-K, *J. geophys. Res.,* **97**(B4), 4489–4495.

Finger, L.W. & Hazen, R.M., 1980. Crystal-structure and isothermal compression of Fe_2O_3,Cr_2O_3, and V_2O_3 to 50 kbars, *J. Appl. Phys.,* **51**(10), 5362–5367.

Fiquet, G., Richet, P. & Montagnac, G., 1999. High-temperature thermal expansion of lime, periclase, corundum and spinel, *Phys. Chem. Miner.,* **27**(2), 103–111.

Fiquet, G., Dewaele, A., Andrault, D., Kunz, M. & Bihan, T.L., 2000. Thermoelastic properties and crystal structure of $MgSiO_3$ perovskite at lower mantle pressure and temperature conditions, *Geophys. Res. Lett.,* **27,** 21–24.

Flesch, L.M., Li, B.S. & Liebermann, R.C., 1998. Sound velocities of polycrystalline $MgSiO_3$-orthopyroxene to 10 GPa at room temperature, *Am. Mineral.,* **83**(5–6), 444–450.

Fortes, A.D., 2018. Accurate and precise lattice parameters of H_2O and D_2O ice Ih between 1.6 and 270 K from high-resolution time-of-flight neutron powder diffraction data, *Acta Crystallogr. Sect. B-Struct. Sci. Cryst. Eng. Mater.,* **74,** 196–216.

Frost, D.J., 2003a. Fe^{2+}-Mg partitioning between garnet, magnesiowustite, and $(Mg,Fe)_2SiO_4$ phases of the transition zone, *Am. Mineral.,* **88**(2–3), 387–397.

Frost, D.J., 2003b. The structure and sharpness of $(Mg,Fe)_2SiO_4$ phase transformations in the transition zone, *Earth planet. Sci. Lett.,* **216**(3), 313–328.

Frost, D.J., Langenhorst, F. & van Aken, P.A., 2001. Fe-Mg partitioning between ringwoodite and magnesiowustite and the effect of pressure, temperature and oxygen fugacity, *Phys. Chem. Miner.,* **28**(7), 455–470.

Gasparik, T., 1984. Experimentally determined stability of clinopyroxene + garnet + corundum in the system $CaO-MgO-Al_2O_3-SiO_2$, *Am. Mineral.,* **69**(11–1), 1025–1035.

Gasparik, T., 1985. Experimental-study of subsolidus phase-relations and mixing properties of pyroxene and plagioclase in the system $Na_2O-CaO-Al_2O_3-SiO_2$, *Contrib. Mineral. Petrol.,* **89**(4), 346–357.

Gasparik, T., 1989. Transformation of enstatite-diopside-jadeite pyroxenes to garnet, *Contrib. Mineral. Petrol.,* **102**(4), 389–405.

Gasparik, T., 1990. A thermodynamic model for the enstatite-diopside join, *Am. Mineral.,* **75**(9–10), 1080–1091.

Gasparik, T., 1992. Enstatite-jadeite join and its role in the earths mantle, *Contrib. Mineral. Petrol.,* **111**(3), 283–298.

Gasparik, T., 1996a. Melting experiments on the enstatite-diopside join at 70-224 kbar, including the melting of diopside, *Contrib. Mineral. Petrol.,* **124**(2), 139–153.

Gasparik, T., 1996b. Diopside-jadeite join at 16-22 GPa, *Phys. Chem. Miner.,* **23**(7), 476–486.

Gasparik, T., 2000. Evidence for the transition zone origin of some Mg,FeO inclusions in diamonds, *Earth planet. Sci. Lett.,* **183**(1–2), 1–5.

Gasparik, T. & Newton, R.C., 1984. The reversed alumina contents of ortho-pyroxene in equilibrium with spinel and forsterite in the system $mgo-Al_2O_3-SiO_2$, *Contrib. Mineral. Petrol.,* **85**(2), 186–196.

Gassmoller, R., Dannberg, J., Bangerth, W., Heister, T. & Myhill, R., 2020. On formulations of compressible mantle convection, *Geophys. J. Int.,* **221**(2), 1264–1280.

Gatta, G.D., Nestola, F. & Walter, J.M., 2006. On the thermo-elastic behaviour of kyanite: a neutron powder diffraction study up to 1200ºC, *Mineral. Mag.,* **70**(3), 309–317.

Gieske, J.H. & Barsch, G.R., 1968. Pressure dependence of elastic constants of single crystalline aluminum oxide, *Phys. Status Solidi,* **29**(1), 121–131.

Gillery, F.H. & Bush, E.A., 1959. Thermal contraction of beta-eucryptite $(LI_2O.AL_2O_3.2SiO_2)$ by X-ray and dilatometer methods, *J. Am. Ceram. Soc.,* **42**(4), 175–177.

Goldsmith, J.R., 1980. The melting and breakdown reactions of anorthite at high-pressures and temperatures, *Am. Mineral.,* **65**(3–4), 272–284.

Grover, J., 1972. The stability of low-clinoenstatite in the system $Mg_2Si_2O_6$-$CaMgSi_2O_6$ (abstract), *EOS, Trans. Am. geophys. Un.,* **53,** 539.

Guignot, N., Andrault, D., Morard, G., Bolfan-Casanova, N. & Mezouar, M., 2007. Thermoelastic properties of post-perovskite phase $MgSiO_3$ determined experimentally at core-mantle boundary P-T conditions, *Earth planet. Sci. Lett.,* **256**(1–2), 162–168.

Hackler, R.T. & Wood, B.J., 1989. Experimental-determination of Fe and Mg exchange between garnet and olivine and estimation of Fe-Mg mixing properties in garnet, *Am. Mineral.,* **74**(9–10), 994–999.

Harlov, D.E. & Milke, R., 2002. Stability of corundum plus quartz relative to kyanite and sillimanite at high temperature and pressure, *Am. Mineral.,* **87**(4), 424–432.

Harrison, R.J., Redfern, S. A.T. & O'Neill, H. S.C., 1998. The temperature dependence of the cation distribution in synthetic hercynite $(FeAl_2O_4)$ from in-situ neutron structure refinements, *Am. Mineral.,* **83**(9–10), 1092–1099.

Haselton, H.T. & Westrum, E.F., 1980. Low-temperature heat-capacities of synthetic pyrope, grossular, and $pyrope_{60 }grossular_{40}$, *Geochim. Cosmochim. Acta,* **44**(5), 701–709.

Haselton, H.T., Hemingway, B.S. & Robie, R.A., 1984. Low-temperature heat-capacities of $CaAl_2SiO_6$ glass and pyroxene and thermal-expansion of $CaAl_2SiO_6$ pyroxene, *Am. Mineral.,* **69**(5–6), 481–489.

Hazen, R.M., Weinberger, M.B., Yang, H.X. & Prewitt, C.T., 2000. Comparative high-pressure crystal chemistry of wadsleyite, beta-$(Mg_{1-x}Fe_x)_{(2)}SiO_4$, with x=0 and 0.25, *Am. Mineral.,* **85**(5–6), 770–777.

Heinz, D.L. & Jeanloz, R., 1983. Inhomogeneity parameter of a homogeneous earth, *Nature,* **301**(5896), 138–139.

Hemingway, B.S., Robie, R.A., Evans, H.T. & Kerrick, D.M., 1991. Heat-capacities and entropies of sillimanite, fibrolite, andalusite, kyanite, and quartz and the Al_2SiO_5 phase-diagram, *Am. Mineral.,* **76**(9–10), 1597–1613.

Hemingway, B.S., Bohlen, S.R., Hankins, W.B., Westrum, E.F. & Kuskov, O.L., 1998. Heat capacity and thermodynamic properties for coesite and jadeite, reexamination of the quartz-coesite equilibrium boundary, *Am. Mineral.,* **83**(5–6), 409–418.

Higo, Y., Inoue, T., Irifune, T., Funakoshi, K.I. & Li, B.S., 2008. Elastic wave velocities of $(Mg_{0.91}Fe_{0.09})_2SiO_4$ ringwoodite under P-T conditions of the mantle transition region, *Phys. Earth planet. Inter.,* **166**(3–4), 167–174.

Hirose, K., 2002. Phase transitions in pyrolitic mantle around 670-km depth: implications for upwelling of plumes from the lower mantle, *J. geophys. Res.,* **107**(B4), 2078.

Hirose, K., Komabayashi, T., Murakami, M. & Funakoshi, K., 2001. In situ measurements of the majorite-akimotoite-perovskite phase transition boundaries in $MgSiO_3$, *Geophys. Res. Lett.,* **28**(23), 4351–4354.

Hirose, K., Takafuji, N., Sata, N. & Ohishi, Y., 2005. Phase transition and density of subducted MORB crust in the lower mantle, *Earth planet. Sci. Lett.,* **237**(1–2), 239–251.

Holland, T. & Powell, R., 2003. Activity-composition relations for phases in petrological calculations: an asymmetric multicomponent formulation, *Contrib. Mineral. Petrol.,* **145**(4), 492–501.

Holland, T.J.B., 1980. Reaction albite = jadeite + quartz determined experimentally in the range 600-1200°C, *Am. Mineral.,* **65**(1–2), 129–134.

Holland, T.J.B., 1983. The experimental determination of activities in disordered and short-range ordered jadeitic pyroxenes, *Contrib. Mineral. Petrol.,* **82**(2–3), 214–220.

Holland, T.J.B. & Powell, R., 1998. An internally consistent thermodynamic data set for phases of petrological interest, *J. Metamor. Geol.,* **16**(3), 309–343.

Holland, T.J.B., Navrotsky, A. & Newton, R.C., 1979. Thermodynamic parameters of $CaMgSi_2O_6$-$Mg_2Si_2O_6$ pyroxenes based on regular solution and cooperative disordering models, *Contrib. Mineral. Petrol.,* **69**(4), 337–344.

Hovis, G.L., Crelling, J., Wattles, D., Dreibelbis, B., Dennison, A., Keohane, M. & Brennan, S., 2003. Thermal expansion of nepheline-kalsilite crystalline solutions, *Mineral. Mag.,* **67**(3), 535–546.

Hovis, G.L., Mott, A. & Roux, J., 2009. Thermodynamic, phase equilibrium, and crystal chemical behavior in the nepheline-kalsilite system, *Am. J. Sci.,* **309**(5), 397–419.

Hu, Y., Dera, P. & Zhuravlev, K., 2015. Single-crystal diffraction and raman spectroscopy of hedenbergite up to 33 GPa, *Phys. Chem. Miner.,* **42**(7), 595–608.

HughJones, D., 1997. Thermal expansion of $MgSiO_3$ and $FeSiO_3$ ortho- and clinopyroxenes, *Am. Mineral.,* **82**(7–8), 689–696.

HughJones, D., Sharp, T., Angel, R. & Woodland, A., 1996. The transition of orthoferrosilite to high-pressure $C2/c$ clinoferrosilite at ambient temperature, *Eur. J. Mineral.,* **8**(6), 1337–1345.

HughJones, D.A. & Angel, R.J., 1997. Effect of Ca^{2+} and Fe^{2+} on the equation of state of $MgSiO_3$ orthopyroxene, *J. geophys. Res.,* **102**(B6), 12 333–12 340.

Ichikawa, H., Kameyama, M., Senshu, H., Kawai, K. & Maruyama, S., 2014. Influence of majorite on hot plumes, *Geophys. Res. Lett.,* **41**(21), 7501–7507.

Imada, S., Hirose, K. & Ohishi, Y., 2011. Stabilities of NAL and Ca-ferrite-type phases on the join $NaAlSiO_4$-$MgAl_2O_4$ at high pressure, *Phys. Chem. Miner.,* **38**(7), 557–560.

Imada, S., Hirose, K., Komabayashi, T., Suzuki, T. & Ohishi, Y., 2012. Compression of $Na_{0.4}Mg_{0.6}Al_{1.6}Si_{0.4}O_4$ NAL and Ca-ferrite-type phases, *Phys. Chem. Miner.,* **39**(7), 525–530.

Irifune, T., 1994. Absence of an aluminous phase in the upper part of the earths lower mantle, *Nature,* **370**(6485), 131–133.

Isaak, D.G., Ohno, I. & Lee, P.C., 2006. The elastic constants of monoclinic single-crystal chrome-diopside to 1,300 K, *Phys. Chem. Miner.,* **32**(10), 691–699.

Ishii, T., Kojitani, H. & Akaogi, M., 2018. Phase relations and mineral chemistry in pyrolitic mantle at 1600-2200°C under pressures up to the uppermost lower mantle: phase transitions around the 660-km discontinuity and dynamics of upwelling hot plumes, *Phys. Earth planet. Inter.,* **274**, 127–137.

Ito, E. & Navrotsky, A., 1985. $MgSiO_3$ ilmenite - calorimetry, phase-equilibria, and decomposition at atmospheric-pressure, *Am. Mineral.,* **70**(9–10), 1020–1026.

Ito, E. & Takahashi, E., 1989. Postspinel transformations in the system Mg_2SiO_4-Fe_2SiO_4 and some geophysical implications, *J. geophys. Res.,* **94**(B8), 10 637–10 646.

Ito, E. & Yamada, H., 1982. Stability relations of silicate spinels, ilmenites, and perovskites, in *High-Pressure Research in Geophysics, Advances in Earth and Planetary Sciences,* pp. 405–420, eds Akimoto, S. & Manghnani, M.H., Center for Academic Publications Japan.

Ito, E., Kubo, A., Katsura, T. & Walter, M.J., 2004. Melting experiments of mantle materials under lower mantle conditions with implications for magma ocean differentiation, *Phys. Earth planet. Inter.,* **143**, 397–406.

Jackson, I., 2007. Properties of rocks and minerals—physical origins of anelasticity and attenuation in rock, in *Treatise on Geophysics,* Vol. 2: Mineral Physics, pp. 493–525, ed. Schubert, G., Elsevier.

Jackson, I. & Niesler, H., 1982. The elasticity of periclase to 3 GPa and some geophysical implications, in *High-Pressure Research in Geophysics,* pp. 93–133, eds Akimoto, S. & Manghnani, M.H., Center for Academic Publications.

Jackson, J.M., Sinogeikin, S.V. & Bass, J.D., 1999. Elasticity of $MgSiO_3$ orthoenstatite, *Am. Mineral.,* **84**(4), 677–680.

Jackson, J.M., Palko, J.W., Andrault, D., Sinogeikin, S.V., Lakshtanov, D.L., Wang, J.Y., Bass, J.D. & Zha, C.S., 2003. Thermal expansion of natural orthoenstatite to 1473 K, *Eur. J. Mineral.,* **15**(3), 469–473.

Jackson, J.M., Sinogeikin, S.V. & Bass, J.D., 2007. Sound velocities and single-crystal elasticity of orthoenstatite to 1073 K at ambient pressure, *Phys. Earth planet. Inter.,* **161**(1-2), 1–12.

Jacobsen, S.D., Reichmann, H.J., Spetzler, H.A., Mackwell, S.J., Smyth, J.R., Angel, R.J. & McCammon, C.A., 2002. Structure and elasticity of single-crystal (Mg,Fe)O and a new method of generating shear waves for gigahertz ultrasonic interferometry, *J. geophys. Res.,* **107**(B2), 2037.

Jamieson, H.E. & Roeder, P.L., 1984. The distribution of Mg and Fe^{2+} between olivine and spinel at 1300°C, *Am. Mineral.,* **69**(3–4), 283–291.

Jiang, F.M., Speziale, S. & Duffy, T.S., 2004. Single-crystal elasticity of grossular- and almandine-rich garnets to 11 GPa by brillouin scattering, *J. geophys. Res.,* **109**(B10),.

Jiang, F.M., Gwanmesia, G.D., Dyuzheva, T.I. & Duffy, T.S., 2009. Elasticity of stishovite and acoustic mode softening under high pressure by brillouin scattering, *Phys. Earth planet. Inter.,* **172**(3-4), 235–240.

Johnson, S.G., 2021. The NLopt nonlinear-optimization package, Available at: http://github.com/stevengj/nlopt.

Jorgensen, J.D., 1978. Compression mechanisms in alpha-quartz structures-SiO_2 and GeO_2, *J. Appl. Phys.,* **49**(11), 5473–5478.

Kandelin, J. & Weidner, D.J., 1988a. The single-crystal elastic properties of jadeite, *Phys. Earth planet. Inter.,* **50**(3), 251–260.

Kandelin, J. & Weidner, D.J., 1988b. Elastic properties of hedenbergite, *J. geophys. Res.,* **93**(B2), 1063–1072.

Karki, B.B. & Crain, J., 1998. First-principles determination of elastic properties of $CaSiO_3$ perovskite at lower mantle pressures, *Geophys. Res. Lett.,* **25**(14), 2741–2744.

Karki, B.B., Warren, M.C., Stixrude, L., Ackland, G.J. & Crain, J., 1997. Ab initio studies of high-pressure structural transformations in silica, *Phys. Rev. B,* **55**, 3465–3471, Erratum ibid. vol. 56, pg. 2884, 1997.

Kato, J., Hirose, K., Ozawa, H. & Ohishi, Y., 2013. High-pressure experiments on phase transition boundaries between corundum, $Rh_2O_3(II)$- and $CaIrO_3$-type structures in Al_2O_3, *Am. Mineral.,* **98**(2-3), 335–339.

Katsura, T., Ueda, Y., Ito, E. & Morooka, K., 1998. Post-spinel transition in Fe_2SiO_4, in *Properties of Earth and Planetary Materials, Geophysical Monograph Series,* pp. 435–440, eds Manghnani, M.H. & Yagi, T., American Geophysical Union.

Katsura, T. *et al.*, 2009. P-V-T relations of the $MgSiO_3$ perovskite determined by in situ X-ray diffraction using a large-volume high-pressure apparatus, *Geophys. Res. Lett.,* **36**(1), doi:10.1029/2008GL035658.

Kennett, B.L.N., 2020. Radial earth models revisited, *Geophys. J. Int.,* **222**(3), 2189–2204.

Kennett, B.L.N., Engdahl, E.R. & Buland, R., 1995. Constraints on seismic velocities in the earth from travel-times, *Geophys. J. Int.,* **122**(1), 108–124.

Khan, A., Connolly, J.A.D. & Olsen, N., 2006. Constraining the composition and thermal state of the mantle beneath Europe from inversion of long-period electromagnetic sounding data, *J. geophys. Res.,* **111**(B10), doi:.

Kiefer, B., Stixrude, L. & Wentzcovitch, R.M., 2002. Elasticity of (Mg,Fe)SiO_3-Perovskite at high pressures, *Geophys. Res. Lett.,* **29**(11), 1539.

Kimizuka, H., Ogata, S., Li, J. & Shibutani, Y., 2007. Complete set of elastic constants of alpha-quartz at high pressure: a first-principles study, *Phys. Rev. B,* **75**(5), 054109.

Klemme, S. & O'Neill, H. S.C., 2000. The near-solidus transition from garnet iherzolite to spinel iherzolite, *Contrib. Mineral. Petrol.,* **138**(3), 237–248.

Kojitani, H., Hisatomi, R. & Akaogi, M., 2007. High-pressure phase relations and crystal chemistry of calcium ferrite-type solid solutions in the system $MgAl_2O_4$-Mg_2SiO_4, *Am. Mineral.,* **92**(7), 1112–1118.

Kojitani, H., Iwabuchi, T., Kobayashi, M., Miura, H. & Akaogi, M., 2011. Structure refinement of high-pressure hexagonal aluminous phases $K_{1.00}Mg_{2.00}Al_{4.80}Si_{1.15}O_{12}$ and $Na_{1.04}Mg_{1.88}Al_{4.64}Si_{1.32}O_{12}$, *Am. Mineral.,* **96**(8-9), 1248–1253.

Kraft, D., 1994. Algorithm 733: TOMP—Fortran modules for optimal-control calculations, *ACM Trans. Math. Softw.,* **20**(3), 262–281.

Krupka, K.M., Robie, R.A. & Hemingway, B.S., 1979. High-temperature heat-capacities of corundum, periclase, anorthite, $CaAl_2Si_2O_8$ glass, muscovite, pyrophyllite, $KAlAi_3O_8$ glass, grossular, and $NaAlSi_3O_8$ glass, *Am. Mineral.,* **64**(1–2), 86–101.

Krupka, K.M., Robie, R.A., Hemingway, B.S., Kerrick, D.M. & Ito, J., 1985. Low-temperature heat-capacities and derived thermodynamic properties of anthophyllite, diopside, enstatite, bronzite, and wollastonite, *Am. Mineral.,* **70**(3–4), 249–260.

Kung, J., Li, B.S., Uchida, T. & Wang, Y.B., 2005. In-situ elasticity measurement for the unquenchable high-pressure clinopyroxene phase: Implication for the upper mantle, *Geophys. Res. Lett.,* **32**(1), L01307.

Levy, D., Artioli, G. & Dapiaggi, M., 2004. The effect of oxidation and reduction on thermal expansion of magnetite from 298 to 1173 K at different vacuum conditions, *J. Solid State Chem.,* **177**(4–5), 1713–1716.

Li, B.S., Liebermann, R.C. & Weidner, D.J., 2001. P-V-Vp-Vs-T measurements on wadsleyite to 7 GPa and 873 K: implications for the 410-km seismic discontinuity, *J. geophys. Res.,* **106**(B12), 30 579–30 591.

Li, L. & Weidner, D.J., 2008. Effect of phase transitions on compressional-wave velocities in the earth's mantle, *Nature,* **454**(7207), 984–986.

Liebermann, R.C. & Schreiber, E., 1968. Elastic constants of polycrystalline hematite as a function of pressure to 3 kilobars, *J. geophys. Res.,* **73**(20), 6585–6590.

Lin, J.F., Degtyareva, O., Prewitt, C.T., Dera, P., Sata, N., Gregoryanz, E., Mao, H.K. & Hemley, R.J., 2004. Crystal structure of a high-pressure/high-temperature phase of alumina by in situ X-ray diffraction, *Nat. Mater.,* **3**(6), 389–393.

Lindsley, D.H., 1983. Pyroxene thermometry, *Am. Mineral.,* **68**(5–6), 477–493.

Liu, H., Caldwell, W.A., Benedetti, L.R., Panero, W. & Jeanloz, R., 2003. Static compression of alpha-fe2o3: linear incompressibility of lattice parameters and high-pressure transformations, *Phys. Chem. Miner.,* **30**(9), 582–588.

Liu, J.C. *et al.*, 2018. Valence and spin states of iron are invisible in earth's lower mantle, *Nat. Commun.,* **9**, 1284.

Liu, X., 2006. Phase relations in the system $KAlSi_3O_8$-$NaAlSi_3O_8$ at high pressure-high temperature conditions and their implication for the petrogenesis of lingunite, *Earth planet. Sci. Lett.,* **246**(3–4), 317–325.

Liu, Z.D., *et al.*, 2017. Phase relations in the system $MgSiO_3$-Al_2O_3 up to 2300k at lower mantle pressures, *J. geophys. Res.,* **122**(10), 7775–7788.

Mao, H.K., Takahashi, T., Bassett, W.A. & Weaver, J.S., 1969. Effect of pressure and temperature on molar volumes of wustite and of 3 $(Fe Mg)_2SiO_4$ spinel solid solutions, *J. geophys. Res.,* **74**(4), 1061–1069.

Marquardt, H., Speziale, S., Reichmann, H.J., Frost, D.J., Schilling, F.R. & Garnero, E.J., 2009. Elastic shear anisotropy of ferropericlase in earth's lower mantle, *Science,* **324**(5924), 224–226.

Masters, G. & Gubbins, D., 2003. On the resolution of density within the earth. *Phys. Earth planet. Inter.,* **140,** 159–167.

Masters, T.G., 1979. Observational constraints on the chemical and thermal structure of the earth's deep interior, *Geophys. J. R. astr. Soc.,* **57,** 507–534.

McCammon, C.A. & Liu, L.G., 1984. The effects of pressure and temperature on nonstoichiometric wustite, fexo - the iron-rich phase-boundary, *Phys. Chem. Miner.,* **10**(3), 106–113.

Milberg, M.E. & Blair, H.D., 1977. Thermal-expansion of cordierite, *Journal of the American Ceramic Society,* **60**(7–8), 372–373.

Mirwald, P.W. & Massone, H.-J., 1980. The low-high quartz and quartz-coesite transition to 40 kbar between 600 and 1600 C and some reconnaissance data on teh effect of $NaAlO_2$ component on the low quartz-coesite transition, *J. geophys. Res.,* **85**(NB12), 6983–6990.

Montagner, J.P. & Kennett, B.L.N., 1996. How to reconcile body-wave and normal-mode reference earth models, *Geophys. J. Int.,* **125**(1), 229–248.

Mookherjee, M., 2011. Mid-mantle anisotropy: elasticity of aluminous phases in subducted MORB, *Geophys. Res. Lett.,* **38**(14), doi:10.1029/2011GL047923.

Mookherjee, M., Karki, B.B., Stixrude, L. & Lithgow-Bertelloni, C., 2012. Energetics, equation of state, and elasticity of NAL phase: potential host

for alkali and aluminum in the lower mantle, *Geophys. Res. Lett.,* **39**(19), doi:10.1029/2012GL053682.

Morishima, H., Kato, T., Suto, M., Ohtani, E., Urakawa, S., Utsumi, W., Shimomura, O. & Kikegawa, T., 1994. The phase-boundary between alpha-mg2sio4 and Beta-Mg_2SiO_4 determined by in-situ X-Ray-Observation, *Science,* **265**(5176), 1202–1203.

Murakami, M., Hirose, K., Ono, S. & Ohishi, Y., 2003. Stability of $CaCl_2$-type and alpha PbO_2-type SiO_2 at high pressure and temperature determined by in-situ X-ray measurements, *Geophys. Res. Lett.,* **30**(5), 1207.

Murakami, M., Sinogeikin, S.V., Bass, J.D., Sata, N., Ohishi, Y. & Hirose, K., 2007. Sound velocity of $MgSiO_3$ post-perovskite phase: a constraint on the D" discontinuity, *Earth planet. Sci. Lett.,* **259**(1–2), 18–23.

Murakami, M., Ohishi, Y., Hirao, N. & Hirose, K., 2009. Elasticity of MgO to 130 GPa: implications for lower mantle mineralogy, *Earth planet. Sci. Lett.,* **277**(1–2), 123–129.

Nabetani, K., *et al.*, 2015. Suppression of temperature hysteresis in negative thermal expansion compound $BiNi_1$-xFexO3 and zero-thermal expansion composite, *Appl. Phys. Lett.,* **106**(6), 5.

Nakagawa, T. & Tackley, P.J., 2004. Effects of a perovskite-post perovskite phase change near core-mantle boundary in compressible mantle convection, *Geophys. Res. Lett.,* **31**(16),.

Nakagawa, T., Tackley, P.J., Deschamps, F. & Connolly, J. A.D., 2009. Incorporating self-consistently calculated mineral physics into thermochemical mantle convection simulations in a 3-D spherical shell and its influence on seismic anomalies in Earth's mantle, *Geochem. Geophys. Geosyst.,* **10**(3), doi:10.1029/2008GC002280.

Nakajima, Y., Frost, D.J. & Rubie, D.C., 2012. Ferrous iron partitioning between magnesium silicate perovskite and ferropericlase and the composition of perovskite in the earth's lower mantle, *J. geophys. Res.,* **117**(B8), doi: 10.1029/2012JB009151.

Nestola, F. & Tribaudino, M., 2003. The structure of pbca orthopyroxenes along the join diopside-enstatite ($CaMgSi_2O_6$-$Mg_2Si_2O_6$), *Eur. J. Mineral.,* **15**(2), 365–371.

Oganov, A.R. & Ono, S., 2005. The high-pressure phase of alumina and implications for Earth's D" layer, *Proc. Natl. Acad. Sci. U.S.A.,* **102**(31), 10 828–10 831.

Ohno, I., Harada, K. & Yoshitomi, C., 2006. Temperature variation of elastic constants of quartz across the alpha-beta transition, *Physics and Chemistry of Minerals,* **33**(1), 1–9.

Ohtani, E., Kagawa, N. & Fujino, K., 1991. Stability of majorite (Mg, Fe)SiO_3 at high-pressures and 1800°C, *Earth planet. Sci. Lett.,* **102**(2), 158–166.

O'Neill, H. S.C., McCammon, C.A., Canil, D., Rubie, D.C., Ross, C.R. & Seifert, F., 1993. Mossbauer-spectroscopy of mantle transition zone phases and determination of minimum Fe-$^{3+}$ content, *Am. Mineral.,* **78**(3–4), 456–460.

Ono, A., Akaogi, M., Kojitani, H., Yamashita, K. & Kobayashi, M., 2009. High-pressure phase relations and thermodynamic properties of hexagonal aluminous phase and calcium-ferrite phase in the systems $NaAlSiO_4$-$MgAl_2O_4$ and $CaAl_2O_4$-$MgAl_2O_4$, *Phys. Earth planet. Inter.,* **174**(1–4), 39–49.

Ono, S., Hirose, K., Murakami, M. & Isshiki, M., 2002. Post-stishovite phase boundary in SiO_2 determined by in situ X-ray observations, *Earth planet. Sci. Lett.,* **197**(3–4), 187–192.

Ono, S., Oganov, A.R., Koyama, T. & Shimizu, H., 2006. Stability and compressibility of the high-pressure phases of Al_2O_3 up to 200 GPa: implications for the electrical conductivity of the base of the lower mantle, *Earth planet. Sci. Lett.,* **246**(3–4), 326–335.

Ono, S., Brodholt, J.P. & Price, G.D., 2008. First-principles simulation of high-pressure polymorphs in $MgAl_2O_4$, *Phys. Chem. Miner.,* **35**(7), 381–386.

Pacalo, R.E.G. & Gasparik, T., 1990. Reversals of the orthoenstatite-clinoenstatite transition at high-pressures and high-temperatures, *J. geophys. Res.,* **95**(B10), 15 853–15 858.

Pacalo, R. E.G., Weidner, D.J. & Gasparik, T., 1992. Elastic properties of sodium-rich majorite garnet, *Geophys. Res. Lett.,* **19**(18), 1895–1898.

Pamato, M.G., Kurnosov, A., Ballaran, T.B., Trots, D.M., Caracas, R. & Frost, D.J., 2014. Hexagonal $Na_{0.41}$ [na0.125mg0.79al0.085]2

[al0.79si0.21]6 O_{12} (NAL phase): crystal structure refinement and elasticity, *Am. Mineral.,* **99**(8-9), 1562–1569.

Perkins, D. & Newton, R.C., 1980. The compositions of coexisting pyroxenes and garnet in the system cao-mgo-al2o3-sio2 at 900-degrees-1,100-degrees-c and high-pressures, *Contrib. Mineral. Petrol.,* **75**(3), 291–300.

Perkins, D., Holland, T.J.B. & Newton, R.C., 1981. The Al_2O_3 contents of enstatite in equilibrium with garnet in the system $MgO-Al_2O_3-SiO_2$ at 15-40-kbar and 900°C-1600°C, *Contrib. Mineral. Petrol.,* **78**(1), 99–109.

Perrillat, J.P., Ricolleau, A., Daniel, I., Fiquet, G., Mezouar, M., Guignot, N. & Cardon, H., 2006. Phase transformations of subducted basaltic crust in the upmost lower mantle, *Phys. Earth planet. Inter.,* **157**(1-2), 139–149.

Piazzoni, A.S., Steinle-Neumann, G., Bunge, H.P. & Dolejs, D., 2007. A mineralogical model for density and elasticity of the earth's mantle, *Geochem. Geophys. Geosyst.,* **8**(11),.

Presnall, D.C., Weng, Y.H., Milholland, C.S. & Walter, M.J., 1998. Liquidus phase relations in the system $MgO-MgSiO_3$ at pressures up to 25 GPa - constraints on crystallization of a molten Hadean mantle, *Phys. Earth planet. Inter.,* **107**(1-3), 83–95.

Putnis, A., 1992. *Introduction to Mineral Sciences,* Cambridge Univ. Press.

Reichmann, H.J. & Jacobsen, S.D., 2004. High-pressure elasticity of a natural magnetite crystal, *Am. Mineral.,* **89**(7), 1061–1066.

Reid, A.F. & Ringwood, A.E., 1968. High-pressure $NaAlO_2$ an alpha-$NaFeO_2$ isotype, *Inorgan. Chem.,* **7**(3), 443–445.

Ricard, Y., Mattern, E. & Matas, J., 2005. Synthetic tomographic images of slabs from mineral physics, in *Earth's Deep Mantle: Structure, Composition, and Evolution,* pp. 283–300, eds Hilst, R.V.D., Bass, J.D., Matas, J. & Trampert, J., American Geophysical Union.

Ricard, Y., Matas, J. & Chambat, F., 2009. Seismic attenuation in a phase change coexistence loop, *Phys. Earth planet. Inter.,* **176**(1–2), 124–131.

Richet, P., Bottinga, Y., Denielou, L., Petitet, J.P. & Tequi, C., 1982. Thermodynamic properties of quartz, cristobalite, and amorphous SiO_2 - drop calorimetry measurements between 1000 K and 1800 K and a review from 0 K to 2000 K, *Geochim. Cosmochim. Acta,* **46**(12), 2639–2658.

Ricolleau, A. & Fei, Y.W., 2016. Equation of state of the high-pressure Fe_3O_4 phase and a new structural transition at 70 GPa, *Am. Mineral.,* **101**(3–4), 719–725.

Ricolleau, A. *et al.*, 2008. Analytical transmission electron microscopy study of a natural MORB sample assemblage transformed at high pressure and high temperature, *Am. Mineral.,* **93**(1), 144–153.

Robie, R.A. & Hemingway, B.S., 1995. *Thermodynamic Properties of Minerals and Related Substances at 298.15 K and 1 Bar (10^5 Pascals) Pressure and at Higher Temperature,* Vol. 2131 of U.S. Geological Survey Bulletin, United States Geological Survey.

Robie, R.A., Hemingway, B.S. & Fisher, J.R., 1978. *Thermodynamic Properties of Minerals and Related Substances at 298.15 K and 1 Bar (10^5) pascals) Pressure and at Higher Temperatures,* U.S. Geological Survey Bulletin, United States Geological Survey.

Rotter, C.A. & Smith, C.S., 1966. Ultrasonic equation of state of iron. I. Low pressure room temperature, *J. Phys. Chem. Solids,* **27**(2), 267–276.

Saikia, A., Frost, D.J. & Rubie, D.C., 2008. Splitting of the 520-kilometer seismic discontinuity and chemical heterogeneity in the mantle, *Science,* **319**(5869), 1515–1518.

Saito, T., 1965. Anomalous thermal expansion of hematite at a high temperature, *Bull. Chem. Soc. Japan,* **38**(11), 2008–2009.

Sakai, T., Dekura, H. & Hirao, N., 2016. Experimental and theoretical thermal equations of state of $MgSiO_3$ post-perovskite at multi-megabar pressures, *Scient. Rep.,* **6**, 22652.

Sang, L.Q. & Bass, J.D., 2014. Single-crystal elasticity of diopside to 14 GPa by brillouin scattering, *Phys. Earth planet. Inter.,* **228**, 75–79.

Schubert, G., Yuen, D.A. & Turcotte, D.L., 1975. Role of phase-transitions in a dynamic mantle, *Geophys. J. R. astr. Soc.,* **42**(2), 705–735.

Shim, S.H. & Duffy, T.S., 2000. Constraints on the P-V-T equation of state of MsSiO₃ perovskite, *Am. Mineral.,* **85**(2), 354–363.

Shim, S.H., Duffy, T.S. & Shen, G.Y., 2000. The stability and P-V-T equation of state of $CaSiO_3$ perovskite in the earth's lower mantle, *J. geophys. Res.,* **105**(B11), 25 955–25 968.

Shim, S.H., Bengtson, A., Morgan, D., Sturhahn, W.G., Cataiii, K., Zhao, J.Y., Lerche, M. & Prakapenka, V., 2009. Electronic and magnetic structures of the postperovskite-type Fe_2O_3 and implications for planetary magnetic records and deep interiors, *Proc. Natl. Acad. Sci. U.S.A.,* **106**(14), 5508–5512.

Shinmei, T., Sanehira, T., Yamazaki, D., Inoue, T., Irifune, T., Funakoshi, K. & Nozawa, A., 2005. High-temperature and high-pressure equation of state for the hexagonal phase in the system $NaAlSiO_4-MgAl_2O_4$, *Phys. Chem. Miner.,* **32**(8–9), 594–602.

Sinogeikin, S.V. & Bass, J.D., 2000. Single-crystal elasticity of pyrope and MgO to 20 GPa by brillouin scattering in the diamond cell, *Phys. Earth planet. Inter.,* **120**(1–2), 43–62.

Sinogeikin, S.V. & Bass, J.D., 2002a. Elasticity of majorite and a majorite-pyrope solid solution to high pressure: implications for the transition zone, *Geophys. Res. Lett.,* **29**(2),.

Sinogeikin, S.V. & Bass, J.D., 2002b. Elasticity of pyrope and majorite-pyrope solid solutions to high temperatures, *Earth planet. Sci. Lett.,* **203**(1), 549–555.

Sinogeikin, S.V., Katsura, T. & Bass, J.D., 1998. Sound velocities and elastic properties of Fe-bearing wadsleyite and ringwoodite, *J. geophys. Res.,* **103**(B9), 20 819–20 825.

Sinogeikin, S.V., Bass, J.D. & Katsura, T., 2001. Single-crystal elasticity of gamma-$(Mg_{0.91}Fe_{0.09})_2SiO_4$ to high pressures and to high temperatures, *Geophys. Res. Lett.,* **28**(22), 4335–4338.

Sinogeikin, S.V., Bass, J.D. & Katsura, T., 2003. Single-crystal elasticity of ringwoodite to high pressures and high temperatures: implications for 520 km seismic discontinuity, *Phys. Earth planet. Inter.,* **136**(1–2), 41–66.

Sinogeikin, S.V., Zhang, J.Z. & Bass, J.D., 2004. Elasticity of single crystal and polycrystalline $MgSiO_3$ perovskite by brillouin spectroscopy, *Geophys. Res. Lett.,* **31**(6), L06620.

Skinner, B.J., 1966. Thermal expansion, in *Handbook of Physical Constants, Geological Society of America Memoir,* pp. 75–95, ed. Clark, S.P., Geological Society of America.

Smyth, J.R. & McCormick, T.C., 1995. Crystallographic data for minerals, in *Mineral Physics and Crystallography: A Handbook of Physical Constants,* pp. 1–17, ed. Ahrens, T.J., American Geophysical Union.

Solomatova, N.V., Jackson, J.M., Sturhahn, W., Wicks, J.K., Zhao, J.Y., Toellner, T.S., Kalkan, B. & Steinhardt, W.M., 2016. Equation of state and spin crossover of (Mg,Fe)O at high pressure, with implications for explaining topographic relief at the core-mantle boundary, *Am. Mineral.,* **101**(5–6), 1084–1093.

Speziale, S., Duffy, T.S. & Angel, R.J., 2004. Single-crystal elasticity of fayalite to 12 GPa, *J. geophys. Res.,* **109**(B12),.

Stackhouse, S., Brodholt, J.P. & Price, G.D., 2005. High temperature elastic anisotropy of the perovskite and post-perovskite Al_2O_3, *Geophys. Res. Lett.,* **32**(13), L13305.

Stackhouse, S., Brodholt, J.P., Dobson, D.P. & Price, G.D., 2006a. Electronic spin transitions and the seismic properties of ferrous iron-bearing $MgSiO_3$ post-perovskite, *Geophys. Res. Lett.,* **33**(12),.

Stackhouse, S., Brodholt, J.P. & Price, G.D., 2006b. Elastic anisotropy of FeSiO₃ end-members of the perovskite and post-perovskite phases, *Geophys. Res. Lett.,* **33**(1),.

Stixrude, L., 1997. Structure and sharpness of phase transitions and mantle discontinuities, *J. geophys. Res.,* **102**(B7), 14 835–14 852.

Stixrude, L., 2007. Properties of rocks and minerals - seismic properties of rocks and minerals, and structure of the earth, in *Treatise on Geophysics,* Vol. **2**, Mineral Physics, pp. 7–32, ed. Price, G.D., Elsevier.

Stixrude, L. & Karki, B., 2005. Structure and freezing of $MgSiO_3$ liquid in earth's lower mantle, *Science,* **310**(5746), 297–299.

Stixrude, L. & Lithgow-Bertelloni, C., 2005a. Thermodynamics of mantle minerals - I. Physical properties, *Geophys. J. Int.,* **162**(2), 610–632.

Stixrude, L. & Lithgow-Bertelloni, C., 2005b. Mineralogy and elasticity of the oceanic upper mantle: origin of the low-velocity zone, *J. geophys. Res.,* **110**(B3),.

Stixrude, L. & Lithgow-Bertelloni, C., 2007. Influence of phase transformations on lateral heterogeneity and dynamics in earth's mantle, *Earth planet. Sci. Lett.,* **263**(1–2), 45–55.

Stixrude, L. & Lithgow-Bertelloni, C., 2011. Thermodynamics of mantle minerals - II. Phase equilibria, *Geophys. J. Int.,* **184**(3), 1180–1213.

Stixrude, L. & Lithgow-Bertelloni, C., 2012. Geophysics of chemical heterogeneity in the mantle, *Ann. Rev. Earth planet. Sci.,* **40**, 569–595.

Stixrude, L., Cohen, R.E. & Singh, D.J., 1994. Iron at high pressure: linearized augmented plane wave calculations in the generalized gradient approximation, *Phys. Rev. B,* **50**, 6442–6445.

Stixrude, L., de Koker, N., Sun, N., Mookherjee, M. & Karki, B.B., 2009. Thermodynamics of silicate liquids in the deep earth, *Earth planet. Sci. Lett.,* **278**(3–4), 226–232.

Stolen, S., Glockner, R., Gronvold, F., Atake, T. & Izumisawa, S., 1996. Heat capacity and thermodynamic properties of nearly stoichiometric wustite from 13 to 450 K, *Am. Mineral.,* **81**(7–8), 973–981.

Sueda, Y., Irifune, T., Sanehira, T., Yagi, T., Nishiyama, N., Kikegawa, T. & Funakoshi, K., 2009. Thermal equation of state of $CaFe_2O_4$-type $MgAl_2O_4$, *Phys. Earth planet. Inter.,* **174**(1–4), 78–85.

Suzuki, A., Ohtani, E. *et al.*, 2000. In situ determination of the phase boundary between wadsleyite and ringwoodite in Mg_2SiO_4, *Geophys. Res. Lett.,* **27**(6), 803–806.

Tackley, P.J., 1995. On the penetration of an endothermic phase-transition By upwellings and downwellings, *J. geophys. Res.,* **100**(B8), 15 477–15 488.

Tackley, P.J., Stevenson, D.J., Glatzmaier, G.A. & Schubert, G., 1993. Effects of an endothermic phase-transition at 670 km depth in a spherical model of convection in the earths mantle, *Nature,* **361**(6414), 699–704.

Tackley, P.J., Stevenson, D.J., Glatzmaier, G.A. & Schubert, G., 1994. Effects of multiple phase-transitions in a 3-dimensional spherical model of convection in earths mantle, *J. geophys. Res.,* **99**(B8), 15 877–15 901.

Takafuji, N., Yagi, T., Miyajima, N. & Sumita, T., 2002. Study on Al_2O_3 content and phase stability of aluminous-$CaSiO_3$ perovskite at high pressure and temperature, *Phys. Chem. Miner.,* **29**(8), 532–537.

Takenaka, K., 2012. Negative thermal expansion materials: technological key for control of thermal expansion, *Sci. Technol. Adv. Mater.,* **13**(1), 11.

Takenaka, K., Okamoto, Y., Shinoda, T., Katayama, N. & Sakai, Y., 2017. Colossal negative thermal expansion in reduced layered Ruthenate, *Nat. Commun.,* **8**,.

Tange, Y., Nishihara, Y. & Tsuchiya, T., 2009. Unified analyses for P-V-T equation of state of MgO: a solution for pressure-scale problems in high P-T experiments, *J. geophys. Res.,* **114**(B03208), doi:10.1029/2008JB005813.

Tateno, S., Hirose, K., Sata, N. & Ohishi, Y., 2005. Phase relations in $Mg_3Al_2Si_3O_{12}$ to 180 GPa: effect of Al on post-perovskite phase transition, *Geophys. Res. Lett.,* **321**(15),.

Tateno, S., Hirose, K., Sata, N. & Ohishi, Y., 2009. Determination of post-perovskite phase transition boundary up to 4400 K and implications for thermal structure in D'' layer, *Earth planet. Sci. Lett.,* **277**(1–2), 130–136.

Thieblot, L., Roux, J. & Richet, P., 1998. High-temperature thermal expansion and decomposition of garnets, *Eur. J. Mineral.,* **10**(1), 7–15.

Thieblot, L., Tequi, C. & Richet, P., 1999. High-temperature heat capacity of grossular ($Ca_3Al_2Si_3O_{12}$), enstatite ($MgSiO_3$), and titanite ($CaTiSiO_5$), *Am. Mineral.,* **84**(5–6), 848–855.

Tribaudino, M., Prencipe, M., Nestola, F. & Hanfland, M., 2001. A $P2_1/c$-$C2/c$ high-pressure phase transition in $Ca_{0.5}Mg_{1.5}Si_2O_6$ clinopyroxene, *Am. Mineral.,* **86**(7–8), 807–813.

Tronnes, R.G. & Frost, D.J., 2002. Peridotite melting and mineral-melt partitioning of major and minor elements at 22-24.5 GPa, *Earth planet. Sci. Lett.,* **197**(1–2), 117–131.

Tsuchiya, T., Tsuchiya, J., Umemoto, K. & Wentzcovitch, R.A., 2004. Phase transition in $MgSiO_3$ perovskite in the earth's lower mantle, *Earth planet. Sci. Lett.,* **224**(3–4), 241–248.

Voller, V.R. & Prakash, C., 1987. A fixed grid numerical modeling methodology for convection diffusion mushy region phase-change problems, *Int. J. Heat Mass Transf.,* **30**(8), 1709–1719.

Wang, F.L., Tange, Y., Irifune, T. & Funakoshi, K., 2012. P-V-T equation of state of stishovite up to mid-lower mantle conditions, *J. geophys. Res.,* **117**(B6), doi:10.1029/2011JB009100.

Wang, J., Bass, J.D. & Kastura, T., 2014. Elastic properties of iron-bearing wadsleyite to 17.7 GPa: implications for mantle mineral models, *Phys. Earth planet. Inter.,* **228**(C), 92–96.

Wang, Y., Weidner, D.J. & Guyot, F., 1996. Thermal equation of state of $CaSiO$ (sub 3) perovskite, *J. geophys.Res.,* **101,** 661–672.

Wang, Y.B., Weidner, D.J., Zhang, J.Z., Gwanrnesia, G.D. & Liebermann, R.C., 1998. Thermal equation of state of garnets along the pyrope-majorite join, *Phys. Earth planet. Inter.,* **105**(1–2), 59–71.

Watt, J.P., Davies, G.F. & Connell, R. J.O., 1976. The elastic properties of composite materials, *Rev. Geophys. Space Phys.,* **14,** 541–563.

Wei, S.S., Shearer, P.M., Lithgow-Bertelloni, C., Stixrude, L. & Tian, D., 2020. Oceanic plateau of the Hawaiin mantle plume head subducted to the uppermost lower mantle, *Science,* **370,** 983–987.

Weidner, D.J. & Ito, E., 1985. Elasticity of $MgSiO_3$ in the ilmenite phase, *Phys. Earth planet. Inter.,* **40**(1), 65–70.

Wood, B.J., 2000. Phase transformations and partitioning relations in peridotite under lower mantle conditions, *Earth planet. Sci. Lett.,* **174**(3–4), 341–354.

Woodland, A.B. & Angel, R.J., 1997. Reversal of the orthoferrosilite-high-p clinoferrosilite transition, a phase diagram for $FeSiO_3$ and implications for the mineralogy of the Earth's upper mantle, *Eur. J. Mineral.,* **9**(2), 245–254.

Workman, R.K. & Hart, S.R., 2005. Major and trace element composition of the depleted MORB mantle (DMM), *Earth planet. Sci. Lett.,* **231**(1–2), 53–72.

Xu, W.B., Lithgow-Bertelloni, C., Stixrude, L. & Ritsema, J., 2008. The effect of bulk composition and temperature on mantle seismic structure, *Earth planet. Sci. Lett.,* **275**(1–2), 70–79.

Yagi, A., Suzuki, T. & Akaogi, M., 1994. High-pressure transitions in the system $KALSi_3O_8$-$NAAlSi_3O_8$, *Phys. Chem. Miner.,* **21**(1-2), 12–17.

Yagi, T., Akaogi, M., Shimomura, O., Suzuki, T. & Akimoto, S., 1987. Insitu observation of the olivine-spinel phase-transformation in Fe_2SiO_4 using synchrotron radiation, *J. geophys. Res.,* **92**(B7), 6207–6213.

Yamada, H., Matsui, Y. & Ito, E., 1983. Crystal-chemical characterization of $NaAlSiO_4$ with the $CaFe_2O_4$ structure, *Mineral. Mag.,* **47**(343), 177–181.

Yang, H.X. & Ghose, S., 1995. High-temperature single-crystal x-ray-diffraction studies of the ortho-proto phase-transition in enstatite, $Mg_2Si_2O_6$ at 1360 K, *Phys. Chem. Miner.,* **22**(5), 300–310.

Ye, Y., Prakapenka, V., Meng, Y. & Shim, S.H., 2017. Intercomparison of the gold, platinum, and MgO pressure scales up to 140GPa and 2500k, *J. geophys. Res.,* **122**(5), 3450–3464.

Zaretsky, J. & Stassis, C., 1987. Lattice dynamics of g-Fe, *Phys. Rev. B,* **35,** 4500–4502.

Zha, C.S., Duffy, T.S., Downs, R.T., Mao, H.K. & Hemley, R.J., 1996. Sound velocity and elasticity of single-crystal forsterite to 16 GPa, *J. geophys. Res.,* **101**(B8), 17 535–17 545.

Zhang, J., Li, B., Utsumi, W. & Liebermann, R.C., 1996. In situ X-ray observations of the coesite stishovite transition: reversed phase boundary and kinetics, *Phys. Chem. Miner.,* **23**(1), 1–10.

Zhang, J.Z. & Herzberg, C., 1994. Melting experiments on anhydrous peridotite KLB-$_1$ from 5.0 to 22.5 GPa, *J. geophys. Res.,* **99**(B9), 17 729–17 742.

Zhang, S., Cottaar, S., Liu, T., Stackhouse, S. & Militzer, B., 2016. High-pressure, temperature elasticity of Fe- and Al-bearing $MgSiO_3$: implications for the earth's lower mantle, *Earth planet. Sci. Lett.,* **434**(C), 264–273.

Zhang, Z.G., Stixrude, L. & Brodholt, J., 2013. Elastic properties of $MgSiO_3$-perovskite under lower mantle conditions and the composition of the deep earth, *Earth planet. Sci. Lett.,* **379**, 1–12.

Zhao, Y.S., VonDreele, R.B., Shankland, T.J., Weidner, D.J., Zhang, J.Z., Wang, Y.B. & Gasparik, T., 1997. Thermoelastic equation of state of jadeite $NaAlSi_2O_6$: an energy-dispersive reitveld refinement study of low symmetry and multiple phases diffraction, *Geophys. Res. Lett.,* **24**(1), 5–8.

Zhou, C.Y., Greaux, S., Nishiyama, N., Irifune, T. & Higo, Y., 2014. Sound velocities measurement on $MgSiO_3$ akimotoite at high pressures and high

temperatures with simultaneous in situ X-ray diffraction and ultrasonic study, *Phys. Earth planet. Inter.,* **228,** 97–105.

Zou, Y.T., Greaux, S., Irifune, T., Li, B.S. & Higo, Y., 2013. Unusual pressure effect on the shear modulus in MgAl$_2$O$_4$ spinel, *J. Phys. Chem. C,* **117**(46), 24 518–24 526.

APPENDIX A: HeFESTo: AVAILABILITY AND ALGORITHMIC IMPROVEMENTS

We have made HeFESTo publicly available on GitHub at https://github.com/stixrude/HeFESToRepository. We have made several algorithmic improvements to HeFESTo, including expanding the scope of the code to include the computation of the thermal expansivity, bulk modulus and heat capacity of multiphase, multicomponent assemblages as described in the main text. In this appendix, we report further improvements including the analytical computation of the Hessian, the inclusion of non-ideal volume of mixing, a generalization of the treatment of the Landau terms, and more efficient and reliable minimization of the Gibbs free energy.

A1 Hessian for the asymmetric regular solution model

We derive explicit results for the asymmetric van Laar theory (Holland & Powell 2003), which is incorporated in HeFESTo. The chemical potential is

$$\mu_i = \mathcal{G}_i - RT \sum_k^{sites} \left(S_{ik} \ln N_k - \sum_j^c s_{ijk} \ln N_{jk} \right) - \sum_{\beta > \alpha} W_{i\alpha\beta} \left(\delta_{i\alpha} - \phi_\alpha \right) \left(\delta_{i\beta} - \phi_\beta \right), \tag{A1}$$

where

$$N_{jk} = \sum_i^{species} s_{ijk} n_i \tag{A2}$$

$$N_k = \sum_j^c N_{jk} \tag{A3}$$

$$S_{ik} = \sum_j^c s_{ijk} \tag{A4}$$

are, respectively, the number of atoms of component j on site k, the total number of atoms on site k and the sum over the stoichiometric coefficients of component j on site k in species i. Note the further relationship between these quantities and eq. (14): $r_{ij} = \sum_k^{sites} s_{ijk}$. Sums over sites and species extend over all sites and species of the phase to which the species i belongs. In the sum over α, β only terms $\beta > \alpha$ are included, that is, each pair interaction is counted once and like terms $\propto W_{i\alpha\alpha}$ are excluded as these are assumed to be contained in $\mathcal{G}_i$. The size-weighted proportion of species α (Holland & Powell 2003)

$$\phi_\alpha = \frac{n_\alpha d_\alpha}{\sum_\gamma n_\gamma d_\gamma}, \tag{A5}$$

where d_α is the size parameter and the sum is over all species in the phase containing species α, the size-weighted interaction parameter

$$W_{i\alpha\beta} = \frac{2 d_i}{d_\alpha + d_\beta} W_{\alpha\beta} \tag{A6}$$

and δ_{ij} is the Kronecker delta.

The Hessian is

$$H_{im} = \left(\frac{\partial \mu_i}{\partial n_m} \right)_{P,T} = -RT \sum_k \left(\frac{S_{ik} S_{mk}}{N_k} - \sum_j^c \frac{s_{ijk} s_{mjk}}{N_{jk}} \right) + \sum_{\beta > \alpha} W_{i\alpha\beta} \left[\frac{\partial \phi_\alpha}{\partial n_m} \left(\delta_{i\beta} - \phi_\beta \right) + \frac{\partial \phi_\beta}{\partial n_m} \left(\delta_{i\alpha} - \phi_\alpha \right) \right], \tag{A7}$$

where the derivatives

$$\frac{\partial \phi_\alpha}{\partial n_m} = \frac{\delta_{\alpha m} d_\alpha}{\sum_\gamma n_\gamma d_\gamma} - \frac{n_\alpha d_\alpha d_m}{\left(\sum_\gamma n_\gamma d_\gamma \right)^2}. \tag{A8}$$

A2 Landau contributions

We now take the reference state, for which the Landau contribution is zero, to be the low temperature, ordered phase, rather than the high-temperature, disordered phase as in our original formulation and that of many other studies (Putnis 1992; Holland & Powell 1998; Stixrude & Lithgow-Bertelloni 2011). We write the Landau contribution to the Gibbs free energy

$$G_L = S_D \left[(T - T_C)(Q^2 - 1) + \frac{1}{3} T_{C0}(Q^6 - 1) \right], \tag{A9}$$

where the order parameter

$$Q^4 = \frac{T_C - T}{T_{C0}} \tag{A10}$$

for $T < T_C$ and $Q = 0$ otherwise. We continue to assume that the transition temperature varies linearly with pressure

$$T_C = T_{C0} + \frac{V_D}{S_D} P. \tag{A11}$$

We derive other thermodynamic properties from pressure and temperature derivatives of $\mathcal{G}_L$. For example, the Landau contribution to the volume and entropy are, respectively

$$V_L(P, T) = \left(\frac{\partial G_L}{\partial P}\right)_T = -V_D(Q^2 - 1) \quad S_L(P, T) = \left(\frac{\partial G_L}{\partial T}\right)_P = -S_D(Q^2 - 1). \tag{A12}$$

The expression for V_L differs from that given in (Stixrude & Lithgow-Bertelloni 2011). The reason is that we have recast the order parameter Q. We note that most studies of Landau transitions focus on isobaric, usually 1 bar conditions. The order parameter is then commonly written as $Q = 1 - T/T_C$ and $T_C = T_{C0}$. But the generalization of the order parameter to encompass a range of pressure is non-unique. The usual formulation implies that $Q = 1$ at $T = 0$ for all pressures. But the structure of the low temperature phase changes with pressure even at zero temperature, and this should be reflected in a variation of Q with pressure at zero temperature. For example, the structure of the low temperature alpha phase of quartz varies with pressure at low temperature in such a way that it becomes increasingly distinct from the high temperature beta form, for example, by narrowing the inter-tetrahedral angle (Jorgensen 1978). In our formulation this is reflected in the increase of Q with increasing pressure at zero temperature (for $V_D/S_D > 0$), and allowing Q to adopt values greater than unity. An inconvenience is that at very high pressure, well outside the stability field of the phase, Q may become very large, with the result that the phase can become artificially restabilized. We mitigate this problem by limiting the maximum value of Q to 2. Our formulation of the order parameter (eq. A10) recovers the usual Q^2 dependence of V_L found in isobaric studies.

We have included Landau contributions for a much greater variety of phases than in (Stixrude & Lithgow-Bertelloni 2011). In addition to quartz and stishovite, we now include Landau contributions for all iron bearing phases, corresponding to the magnetic disordering transitions either observed, or expected in these phases.

A3 Pressure dependent regular solution

We have generalized our treatment of the non-ideal contributions to the chemical potentials by allowing for pressure dependence of the regular solution parameters W_{ij}. We assume the linear form

$$W_{\alpha\beta}(P) = W_{\alpha\beta}^0 + PV_{\alpha\beta} \tag{A13}$$

and that the $V_{\alpha\beta}$ are independent of pressure and temperature. The partial molar volume of species i is the pressure derivative of eq. (A1)

$$\bar{\mathcal{V}}_i = \left(\frac{\partial \mu_i}{\partial P}\right)_{P,\bar{n}} = \mathcal{V}_i - \sum_{\beta > \alpha} V_{i\alpha\beta} \left(\delta_{i\alpha} - \phi_\alpha\right)\left(\delta_{i\beta} - \phi_\beta\right) \tag{A14}$$

with

$$V_{i\alpha\beta} = \frac{2d_i}{d_\alpha + d_\beta} V_{\alpha\beta}. \tag{A15}$$

A4 Gibbs free energy minimization

We have modified our previous Gibbs free energy minimization algorithm by replacing the quasi-Newton method with that of sequential least-squares quadratic programming (SLSQP, Kraft 1994) as coded in the publicly available package nlopt (Johnson 2021). We find that SLSQP is more efficient than quasi-Netwon: the minimum Gibbs free energy assemblage is found in fewer iterations. In Figs (A1,A2) we show the same tests of efficiency that we presented in our previous paper (Stixrude & Lithgow-Bertelloni 2011). SLSQP also provides more straightforward implementation of the non-negativity constraint (Stixrude & Lithgow-Bertelloni 2011). Otherwise, we continue to follow the numerical strategy outlined in Stixrude & Lithgow-Bertelloni (2011), including by imposing the constraint of fixed bulk composition via minimizing over the null-space of the linear problem (eq. 14), explicitly removing species and phases with vanishingly small abundances, and adding phases according to the chemical affinity criterion.

The greatest advantage of SLSQP is its reliability. No non-linear multidimensional minimization algorithm is perfect and finding the global minimum in $\mathcal{G}$ cannot be guaranteed by any algorithm. Nevertheless, the number of failures is now vanishingly small. Our results for the thermal expansivity, heat capacity, and bulk modulus (Figs 4–7) provide a stringent and convenient test of failure which would appear as irregularities in the variation of these quantities with pressure or temperature.
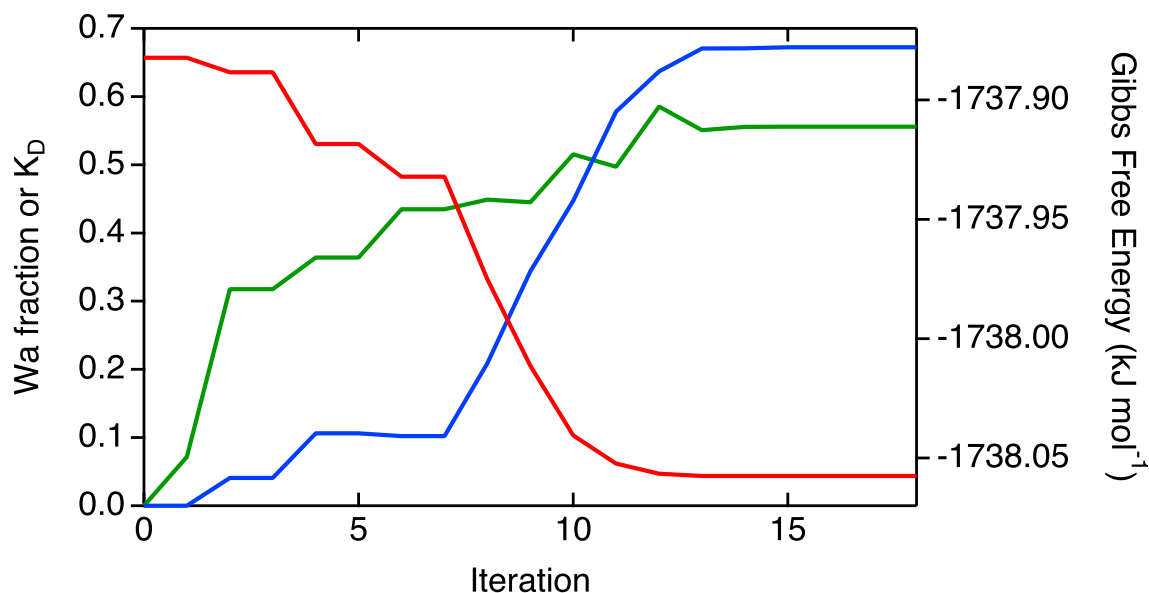
Figure A1. Evolution of (blue) wa fraction (green) the partition coefficient $K = n_{fa}n_{mgwa}/n_{fo}n_{fewa}$ and (red, right-hand axis) the Gibbs free energy with SLSQP iterations. Olivine is adopted as the initial guess to the phase equilibria at conditions within the ol-wa phase coexistence loop at 12.95 GPa and 1500 K and with bulk $X_{Fe} = 0.1$.
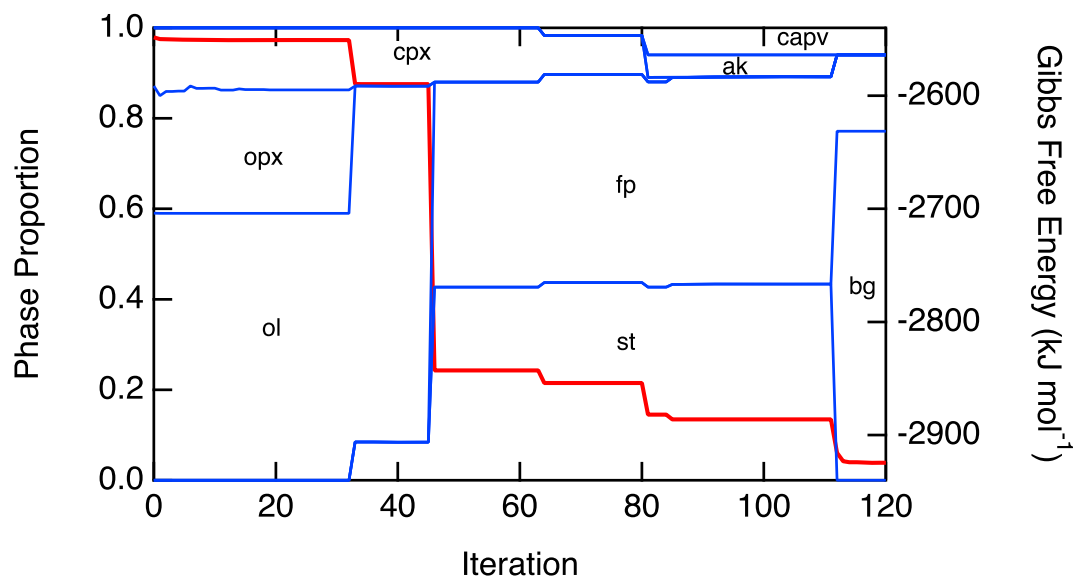
Figure A2. Evolution of (blue) phase proportions and (red, right-hand axis) the Gibbs free energy with SLSQP iterations for a pyrolitic composition (Workman & Hart 2005) for which plg+opx+cpx+ol is adopted as the initial guess to the phase equilbria at lower mantle conditions (40 GPa, 1600 K).

APPENDIX B: NEW PARAMETER SET

We performed a new global inversion of all parameters based on the approach described in our previous publications (Stixrude & Lithgow-Bertelloni 2005b, 2011) and based on new results from experiment and first principles theory (Tables A1–A5). We have also made several changes and additions to the list of species and phases considered as described below. The new parameter set is publicly available at https://github.com/stixrude/HeFESTo_Parameters_010121. Some of the improvements that are contained in this new parameter set also appeared in an intermediate parameter set, which we described briefly in Wei *et al.* (2020), and which is also publicly available at https://github.com/stixrude/HeFESTo_Parameters_270914.

We replaced the Na-bearing end-member of the garnet phase with one of Na-majorite composition. In our previous work, we chose a Na end-member of jadeite composition, which disagrees with results from crystallography and phase equilibria. Crystallography shows that sodium substitution occurs via $^{VIII}Mg^{2+} + {}^{VI}Al^{3+} \rightarrow {}^{VIII}Na^{1+} + {}^{VI}Si^{4+}$, yielding the end-member sodium composition of Na-majorite $Na_2Mg_1Si_5O_{12}$ (Bindi *et al.* 2011). Our new choice agrees with the experimentally observed topology of phase diagrams along the $Mg_2Si_2O_6 - NaAlSi_2O_6$ and $CaMgSi_2O_6 - NaAlSi_2O_6$ joins, which show that garnet stability is limited to half of the bulk compositional range on these two joins (Fig. A3).

Table A1. Properties of mantle species.

Phase	Species	Formula	$\mathcal{F}_0$ (kJ mol⁻¹)	V_0 (cm³ mol⁻¹)	K_{T0} GPa	K'_{T0}	θ_0 K	γ_0	q_0	G_0 GPa	G'_0	η_{S0}	Ref.
feldspar (plg)	Anorthite (an)	$Ca[Al_2Si_2]O_8$	−4013 (4)	100.61	84 (5)	6.7 (10)	752 (2)	0.38 (5)	1.0 (10)	40 (3)	1.1 (5)	1.6 (10)	1–6
feldspar	Albite (ab)	$Na[AlSi_3]O_8$	−3720 (4)	100.45	60 (5)	2.8 (10)	720 (12)	0.58 (3)	1.0 (10)	36 (5)	1.4 (5)	1.0 (10)	1,6–8
spinel (sp)	Spinel (sp)	$(Mg_3Al)(Al_7Mg)O_{16}$	−8680 (22)	159.05	195 (1)	4.6 (1)	856 (23)	0.98 (4)	4.1 (6)	109 (0)	0.6 (0)	2.4 (3)	1.9–11
spinel	Hercynite (hc)	$(Fe_3Al)(Al_7Fe)O_{16}$	−7356 (35)	163.37	209 (2)	4.6 (10)	794 (34)	1.19 (7)	4.1 (10)	84 (13)	0.6 (5)	2.5 (10)	1,2,12
olivine (ol)	Forsterite (fo)	Mg_2SiO_4	−2055 (2)	43.60	128 (2)	4.2 (2)	809 (1)	0.99 (3)	2.1 (2)	82 (2)	1.5 (1)	2.3 (1)	1,13–16
olivine	Fayalite (fa)	Fe_2SiO_4	−1372 (1)	46.29	136 (1)	4.9 (1)	619 (2)	1.08 (7)	2.9 (2)	51 (0)	0.9 (1)	1.7 (2)	1,6,14,16,17
wadsleyite (wa)	Mg-Wadsleyite (mgwa)	Mg_2SiO_4	−2028 (2)	40.52	169 (2)	4.1 (1)	845 (8)	1.20 (9)	2.2 (10)	112 (2)	1.5 (0)	2.6 (3)	1,6,18–21
wadsleyite	Fe-Wadsleyite (fewa)	Fe_2SiO_4	−1358 (7)	42.80	169 (13)	4.1 (10)	647 (21)	1.20 (30)	2.2 (10)	72 (12)	1.5 (5)	1.0 (10)	18,22
ringwoodite (ri)	Mg-Ringwoodite (mgri)	Mg_2SiO_4	−2017 (2)	39.49	185 (2)	4.2 (2)	875 (8)	1.11 (10)	2.4 (4)	123 (2)	1.4 (1)	2.3 (5)	1,6,23–25
ringwoodite	Fe-Ringwoodite (feri)	Fe_2SiO_4	−1359 (3)	41.86	213 (7)	4.2 (10)	663 (9)	1.27 (23)	2.4 (10)	92 (10)	1.4 (5)	1.8 (10)	23,26,27
orthopyroxene (opx)	Enstatite (en)	$MgMgSi_2O_6$	−2914 (2)	62.68	107 (2)	7.0 (4)	812 (4)	0.78 (4)	3.4 (4)	77 (1)	1.5 (1)	2.5 (1)	1,28–33
orthopyroxene	Ferrosilite (fs)	$FeFeSi_2O_6$	−2228 (4)	65.94	101 (4)	7.9 (0)	683 (11)	0.72 (8)	3.4 (10)	52 (5)	1.5 (5)	1.1 (10)	1,2,28,34,35
orthopyroxene	Mg-Tschermaks (mgts)	$MgAl[SiAl]O_6$	−3002 (9)	59.14	107 (10)	7.0 (10)	784 (24)	0.78 (30)	3.4 (10)	93 (10)	1.5 (5)	2.4 (10)	1,2
orthopyroxene	Ortho-Diopside (odi)	$CaMgSi_2O_6$	−3016 (3)	68.05	107 (10)	7.0 (10)	745 (9)	0.78 (30)	3.4 (10)	58 (10)	1.5 (5)	1.3 (10)	1
clinopyroxene (cpx)	Diopside (di)	$CaMgSi_2O_6$	−3030 (2)	66.04	114 (1)	4.8 (2)	783 (3)	1.01 (5)	0.6 (3)	73 (0)	1.7 (1)	1.1 (3)	1,6,14,36,37
clinopyroxene	Hedenbergite (he)	$CaFeSi_2O_6$	−2677 (45)	67.87	119 (4)	4.8 (3)	702 (2)	0.97 (6)	0.6 (10)	61 (1)	1.7 (5)	1.0 (10)	1,6,14,38,39
clinopyroxene	Clinoenstatite (cen)	$MgMgSi_2O_6$	−2907 (3)	62.50	114 (10)	4.8 (10)	807 (8)	1.01 (30)	0.6 (10)	77 (10)	1.7 (5)	1.4 (10)	40
clinopyroxene	Ca-Tschermaks (cats)	$CaAl(SiAl)O_6$	−3119 (5)	63.57	114 (10)	4.8 (10)	804 (5)	0.82 (0)	0.6 (10)	74 (10)	1.7 (5)	1.7 (10)	41,42
clinopyroxene	Jadeite (jd)	$NaAlSi_2O_6$	−2855 (3)	60.51	142 (2)	4.8 (10)	821 (12)	0.90 (8)	0.8 (14)	85 (2)	1.7 (5)	1.9 (10)	1,6,43–45
HP-clinopyroxene (hpcpx)	HP-Clinoenstatite (hpcen)	$Mg_2Si_2O_6$	−2905 (3)	60.76	116 (1)	6.2 (3)	823 (6)	1.12 (5)	0.2 (5)	88 (1)	1.8 (1)	2.1 (5)	46
HP-clinopyroxene	HP-Clinoferrosilite (hpcfs)	$Fe_2Si_2O_6$	−2224 (4)	63.85	116 (10)	6.2 (10)	699 (11)	1.12 (30)	0.2 (10)	75 (10)	1.8 (5)	1.0 (10)	1,47
Ca-perovskite (capv)	Ca-Perovskite (capv)	$CaSiO_3$	−1460 (7)	27.45	236 (4)	3.9 (2)	799 (39)	1.89 (7)	0.9 (16)	155 (12)	2.2 (5)	1.2 (10)	48–51
akimotoite (ak)	Mg-Akimotoite (mgak)	$MgSiO_3$	−1410 (7)	26.35	211 (4)	5.2 (0)	933 (11)	1.19 (13)	2.2 (1)	132 (8)	1.8 (0)	3.4 (3)	1,6,52,53
akimotoite	Fe-Akimotoite (feak)	$FeSiO_3$	−1048 (21)	26.85	211 (10)	5.2 (10)	781 (103)	1.19 (30)	2.2 (10)	161 (10)	1.8 (5)	3.4 (10)	1
akimotoite	Corundum (co)	$AlAlO_3$	−1582 (1)	25.58	253 (5)	3.9 (2)	932 (3)	1.31 (4)	1.7 (2)	163 (2)	1.8 (5)	2.6 (7)	1,6,14,16,54,55
garnet (gt,mj)	Pyrope (py)	$Mg_3AlAlSi_3O_{12}$	−5937 (10)	113.08	170 (2)	4.1 (3)	823 (4)	1.01 (6)	1.4 (5)	94 (2)	1.4 (2)	1.0 (3)	1,14,60–62
garnet	Almandine (al)	$Fe_3AlAlSi_3O_{12}$	−4933 (29)	115.43	174 (2)	4.9 (2)	741 (5)	1.06 (6)	1.4 (10)	96 (1)	1.4 (1)	2.1 (10)	1,14,61,63
garnet	Grossular (gr)	$Ca_3AlAlSi_3O_{12}$	−6275 (11)	125.12	167 (1)	3.9 (2)	823 (2)	1.05 (6)	1.9 (2)	109 (4)	1.2 (1)	2.4 (1)	1,16,30,61,63,64
garnet	Mg-Majorite (mgmj)	$Mg_3MgSiSi_3O_{12}$	−5693 (9)	114.32	165 (3)	4.2 (3)	822 (4)	0.98 (7)	1.5 (5)	85 (2)	1.4 (2)	1.0 (3)	1,14,24,62,65,66
garnet	Na-Majorite (namj)	$(Na_2Mg)MgSiSi_3O_{12}$	−5303 (27)	110.84	172 (3)	5.2 (6)	845 (28)	1.25 (5)	0.1 (12)	115 (1)	1.4 (5)	2.5 (10)	67–69
quartz (qtz)	Quartz (qtz)	SiO_2	−860 (1)	22.42	61 (1)	19.8 (1)	884 (33)	−0.04 (6)	1.0 (10)	45 (1)	0.0 (1)	2.4 (10)	1,70–73
coesite (coes)	Coesite (coes)	SiO_2	−856 (1)	20.66	104 (1)	2.9 (1)	880 (16)	0.29 (3)	1.0 (10)	62 (0)	0.5 (1)	2.8 (10)	1,74,75
stishovite (st)	Stishovite (st)	SiO_2	−817 (1)	14.02	306 (8)	4.0 (1)	1092 (13)	1.56 (6)	2.2 (20)	228 (12)	1.9 (1)	4.4 (10)	1,76–78
seifertite (seif)	Seifertite (seif)	SiO_2	−793 (2)	13.67	327 (2)	4.0 (1)	1129 (17)	1.56 (30)	2.2 (10)	227 (2)	1.8 (1)	4.6 (10)	40,77
bridgmanite (bg)	Mg-Bridgmanite (mgbg)	$MgSiO_3$	−1362 (2)	24.45	251 (3)	4.1 (1)	880 (6)	1.54 (5)	0.8 (4)	173 (2)	1.7 (0)	1.7 (4)	1,48,79–83
bridgmanite	Fe-Bridgmanite (febg)	$FeSiO_3$	−1003 (5)	25.32	271 (10)	4.0 (1)	747 (24)	1.54 (30)	0.8 (10)	130 (40)	1.4 (0)	2.1 (10)	84–87
bridgmanite	Al-Bridgmanite (albg)	$AlAlO_3$	−1518 (3)	24.94	242 (10)	4.1 (5)	858 (9)	1.54 (30)	0.8 (10)	169 (10)	1.6 (1)	2.3 (5)	88–91
post-perovskite (ppv)	Mg-Post-Perovskite (mppv)	$MgSiO_3$	−1314 (3)	23.53	292 (1)	3.7 (1)	941 (8)	1.77 (7)	2.0 (3)	171 (4)	1.9 (1)	1.3 (3)	1,97–100
post-perovskite	Fe-Post-Perovskite (fppv)	$FeSiO_3$	−982 (15)	24.65	292 (10)	3.7 (10)	794 (35)	1.77 (30)	2.0 (10)	130 (5)	1.3 (1)	1.7 (10)	86,101
post-perovskite	Al-Post-Perovskite (appv)	$AlAlO_3$	−1336 (4)	23.85	249 (20)	4.0 (1)	723 (8)	1.89 (2)	2.0 (10)	92 (10)	1.8 (1)	2.5 (2)	91,102,103
ferropericlase (fp)	Periclase (pe)	$Mg_2Mg_2O_4$	−2278 (1)	44.98	161 (3)	3.9 (0)	771 (38)	1.45 (6)	1.5 (1)	131 (1)	2.1 (1)	2.6 (2)	1,6,14,16,60,105–10
ferropericlase	Wüstite (wu)	$Fe_2Fe_2O_4$	−975 (5)	49.02	161 (3)	4.0 (2)	454 (83)	1.45 (30)	1.5 (10)	59 (1)	1.4 (1)	0.1 (10)	14,108–112
ferropericlase	a-NaAlO₂ (anao)	$Na_2Al_2O_4$	−2115 (25)	45.42	161 (10)	3.9 (10)	753 (74)	1.45 (30)	1.5 (10)	108 (10)	2.1 (5)	0.8 (10)	113
Ca-ferrite (cf)	Mg-Ca-Ferrite (mgcf)	$MgAlAlO_4$	−2123 (4)	36.14	213 (6)	4.1 (3)	831 (16)	1.57 (11)	1.0 (10)	130 (10)	1.9 (0)	1.3 (10)	116–121
Ca-ferrite	Fe-Ca-Ferrite (fecf)	$FeAlAlO_4$	−1774 (21)	37.22	213 (10)	4.1 (10)	734 (54)	1.57 (30)	1.0 (10)	160 (10)	1.9 (5)	2.3 (10)	40
Ca-ferrite	Na-Ca-Ferrite (nacf)	$NaAlSiO_4$	−1835 (5)	36.27	220 (1)	4.1 (1)	683 (17)	1.57 (30)	1.0 (10)	135 (1)	1.9 (5)	1.4 (10)	122–124
NAL–phase (nal)	Mg-NAL-Phase (mnal)	$NaMg_2(Al_5Si)O_{12}$	−6167 (15)	109.88	204 (2)	4.3 (1)	858 (18)	1.43 (5)	1.0 (10)	129 (1)	1.7 (0)	1.9 (10)	118,121,126–128

Table A1. Continued

Phase	Species	Formula	$\mathcal{F}_0$ (kJ mol⁻¹)	V_0 (cm³ mol⁻¹)	K_{T0} GPa	K'_{T0}	θ_0 K	γ_0	q_0	G_0 GPa	G'_0	η_{S0}	Ref.
NAL-phase	Fe-NAL-Phase (fnal)	$NaFe_2(Al_5Si)O_{12}$	−5475 (74)	112.05	204 (10)	4.3 (10)	795 (80)	1.43 (30)	1.0 (10)	150 (10)	1.7 (5)	2.7 (10)	129
NAL-phase	Na-NAL-Phase (nnal)	$NaNa_2(Al_5Si_3)O_{12}$	−5567 (42)	109.40	204 (10)	4.3 (10)	850 (51)	1.43 (30)	1.0 (10)	144 (10)	1.7 (5)	2.4 (10)	130
kyanite (ky)	Kyanite (ky)	Al_2SiO_5	−2446 (4)	44.23	160 (1)	4.0 (0)	943 (8)	0.93 (7)	1.0 (10)	118 (10)	1.7 (5)	2.9 (10)	1,131–133
nepheline (neph)	Nepheline (neph)	$NaAlSiO_4$	−1994 (21)	53.87	53 (1)	4.0 (10)	744 (13)	0.70 (2)	1.0 (10)	31 (1)	1.3 (5)	0.6 (10)	2,14,134,135

Notes: 1. Smyth & McCormick (1995) 2. Bass (1995) 3. Angel et al. (1988) 4. Krupka et al. (1979) 5. Robie et al. (1978) 6. Fei (1995) 7. Brown et al. (2006) 8. Downs & Palmer (1994) 9. Zou et al. (2013) 10. Fiquet et al. (1999) 11. Anderson & Isaak (1995) 12. Harrison et al. (1998) 13. Zha et al. (1996) 14. Robie & Hemingway (1995) 15. Bouhifd et al. (1996) 16. Anderson & Isaak (1995) 17. Speziale et al. (2004) 18. Sinogeikin et al. (1998) 19. Wang et al. (2014) 20. Fei et al. (1992) 21. Li et al. (2001) 22. Hazen et al. (2000) 23. Sinogeikin et al. (2003) 24. Higo et al. (2008) 25. Sinogeikin et al. (2001) 26. O'Neill et al. (1993) 27. Mao et al. (1969) 28. Jackson et al. (1999) 29. Flesch et al. (1998) 30. Thieblot et al. (1999) 31. Krupka et al. (1985) 32. Jackson et al. (2003) 33. Jackson et al. (2007) 34. HughJones & Angel (1997) 35. HughJones et al. (1997) 36. Sang & Bass (2014) 37. Isaak et al. (2006) 38. Kandelin & Weidner (1988b) 39. Hu et al. (2015) 40. This work (2010) 41. Haselton et al. (1984) 42. Etzel et al. (2007) 43. Kandelin & Weidner (1988a) 44. Hemingway et al. (1998a) 45. Zhao et al. (1997) 46. Kung et al. (2005) 47. HughJones et al. (1996) 48. Shim & Duffy (2000) 49. Shim et al. (2000) 50. Wang et al. (1996) 51. Karki & Crain (1998) 52. Weidner & Ito (1985) 53. Zhou et al. (2014) 54. Gieske & Barsch (1968) 55. Dewaele & Torrent (2013) 56. Finger & Hazen (1980) 57. Liebermann & Schreiber (1968) 58. Liu et al. (2003) 59. Saito (1965) 60. Sinogeikin & Bass (2000) 61. Thieblot et al. (1998) 62. Sinogeikin & Bass (2002b) 63. Jiang et al. (2004) 64. Haselton & Westrum (1980) 65. Sinogeikin & Bass (2002a) 66. Wang et al. (1998) 67. Bindi et al. (2011) 68. Pacalo et al. (1992) 69. Dymshits et al. (2014) 70. Ohno et al. (2006) 71. Kimizuka et al. (2007) 72. Richet et al. (1982) 73. Ackerman & Sorrell (1974) 74. Chen et al. (2015) 75. Bourova et al. (2006) 76. Jiang et al. (2009) 77. Karki et al. (1997) 78. Wang et al. (2012) 79. Sinogeikin et al. (2004) 80. Murakami et al. (2007) 81. Fiquet et al. (2000) 82. Katsura et al. (2009) 83. Zhang et al. (2013) 84. Dorfman et al. (2013) 85. Kiefer et al. (2002) 86. Dorfman & Duffy (2014) 87. Stackhouse et al. (2006a) 88. Oganov & Ono (2005) 89. Lin et al. (2004) 90. Duan et al. (1999) 91. Stackhouse et al. (2005) 92. Liu et al. (2018) 93. Bykova et al. (2016) 94. This work (2019) 95. This work (2016) 96. This work (2020) 97. Sakai et al. (2016) 98. Zhang et al. (2016) 99. Zhang et al. (2007) 100. Tsuchiya et al. (2004) 101. Stackhouse et al. (2006b) 102. Ono et al. (2006) 103. Caracas & Cohen (2005) 104. Shim et al. (2009) 105. Jackson & Niesler (1982) 106. Murakami et al. (2009) 107. Dorogokupets & Dewaele (2007) 108. McCammon & Liu (1984) 109. Solomatova et al. (2016) 110. Stolen et al. (1996) 111. Jacobsen et al. (2002) 112. Marquardt et al. (2009) 113. Reid & Ringwood (1968) 114. Reichmann & Jacobsen (2004) 115. Levy et al. (2004) 116. Kojitani et al. (2007) 117. Sueda et al. (2009) 118. Imada et al. (2012) 119. Skinner (1966) 120. This work (2013) 121. Dai et al. (2013) 122. Yamada et al. (1983) 123. Dubrovinsky et al. (2002) 124. Mookherjee (2011) 125. Ricolleau & Fei (2016) 126. Kojitani et al. (2011) 127. Pamato et al. (2014) 128. Shinmei et al. (2005) 129. This work (2014) 130. Mookherjee (2012) 131. Comodi et al. (1997) 132. Hemingway et al. (1991) 133. Gatta et al. (2006) 134. Hovis et al. (2009) 135. Adams et al. (2006) 136. Hovis et al. (2003) 137. Rotter & Smith (1966) 138. Basinski et al. (1955) 139. Stixrude et al. (1994) 140. Zaretsky & Stassis (1987) 141. Dewaele et al. (2006) 142. Antonangeli & Ohtani (2015).

Table A2. Interaction parameters[1]

Phase	Species 1	Species 2	W_{12}^0 (kJ mol^{-1})	Ref.[2]
plg	an	ab	13 (2)	Holland & Powell (2003)
sp	sp	hc	− 0.5 (90)	
ol	fo	fa	4.7 (21)	
wa	mgwa	fewa	13.2 (25)	
ri	mgri	feri	7.6 (17)	
opx	en	odi	32.2 (10)	
opx	fs	odi	32.2 (10)	3
opx	mgts	odi	48 (11)	
cpx	di	cen	24.7 (20)	Holland *et al.* (1979)
cpx	di	cats	26 (4)	Benisek *et al.* (2007)
cpx	di	jd	24.3 (20)	Holland (1983)
cpx	he	cen	24.7 (20)	3
cpx	he	cats	26 (4)	3
cpx	he	jd	24.3 (20)	3
cpx	cen	cats	60.1 (88)	
cpx	cen	jd	46.0 (45)	
cpx	cats	jd	10 (4)	Cohen (1986)
ak	mgak	co	59.3 (64)	
ak	feak	co	59.3 (64)	3
gt	py	gr	21.1 (71)	
gt	py	mgmj	22.7 (69)	
gt	py	namj	22.7 (69)	4
gt	al	gr	21.1 (71)	3
gt	al	mgmj	22.7 (69)	3
gt	gr	mgmj	61 (17)	
gt	gr	namj	61 (17)	4
gt	mgmj	namj	71 (15)	
bg	mgbg	febg	− 11.4 (18)	
bg	mgbg	albg	35.0 (35)	
ppv	mppv	fppv	− 11.0 (35)	
ppv	mppv	appv	35.0 (100)	5
ppv	fppv	appv	35.0 (100)	3
fp	pe	wu	44.0 (4)	Frost (2003a)
fp	pe	anao	120 (40)	
fp	wu	anao	120 (40)	3
cf	mgcf	nacf	61 (12)	
cf	fecf	nacf	61 (12)	3
nal	mnal	nnal	− 61 (12)	
nal	fnal	nnal	− 61 (12)	3

Notes: 1. Size parameters $d_\alpha = 1$ for all species except $d_{cats} = 3.50$ and $d_{nacf} = 4.06$. Non-ideal volume parameters $V_{12} = 0$ for all species except $V_{py-gr} = 1.03$ cm^3 mol^{-1} (Bosenick & Geiger 1997) and $V_{pe-wu} = 0.44$ cm^3 mol^{-1} (Frost 2003a). 2. From our global inversion of phase equilibria unless otherwise noted. 3. Assumed to be the same as the interaction with the magnesian end-member, for example $W_{fs-odi} = W_{en-odi}$. 4. Assumed the same as the interaction with mgmj, for example $W_{py-mgmj} = W_{py-namj}$. 5. Assumed to be the same as the corresponding interaction in *bg*, for example $W_{mgbg-albg} = W_{mppv-appv}$.

We have added the NaAlO$_2$ end-member to the ferropericlase phase. This addition agrees with observations from experiment and from natural samples that ferropericlase accepts sodium in mantle-like bulk compositions (Brey *et al.* 2004; Gasparik 2000; Wood 2000; Irifune 1994; Hirose 2002). In fact, experiments show that ferropericlase is the dominant host of Na in the lower mantle in peridotitic compositions. Results of HeFESTo agree reasonably well with experimental observations of the Na content of ferropericlase in a variety of bulk compositions (Fig. A4). The addition of the NaAlO$_2$ end-member to ferropericlase is also important because it yields agreement with experimental observations of phase equilibria in peridotitic compositions. Ferropericlase provides a host for Na in the lower mantle other than the *cf* phase which, in our previous parameter set, was the only Na-bearing phase in the lower mantle and which was therefore present throughout the lower mantle for bulk compositions that contained Na, in disagreement with experimental observations that find no *cf* in peridotitic bulk compositions at typical lower mantle temperatures. With our new parameter set, we find no *cf* in the lower mantle in peridotite (Fig. 4).

We have added the sodium-aluminum rich phase (nal); which is an important lower mantle phase, especially in basaltic compositions in the shallow lower mantle (Perrillat *et al.* 2006; Ricolleau *et al.* 2008). Experiments show that *nal* and *cf* may coexist in basaltic compositions,

Table A3. Landau parameters.

Species	T_{C0} (K)	S_D (J mol^{-1} K^{-1})	V_D (cm^3 mol^{-1})	Ref.[1]
hc[2]	5.00	53.53	0.00	
fa	65.00	26.76	0.00	Aronson *et al.* (2007)
fewa	5.00	26.76	0.00	
feri	5.00	26.76	0.00	
fs	5.00	26.76	0.00	
he	5.00	13.38	0.00	
fec2	5.00	26.76	0.00	
feil	5.00	13.38	0.00	
al	7.50	40.14	0.00	Anovitz *et al.* (1993)
qtz	847.00	5.76	1.36	Mirwald & Massone (1980)
st[3]	−4250	0.001	0.012	Andrault *et al.* (1998); Ono *et al.* (2002)
febg	5.00	13.38	0.00	
fppv	5.00	13.38	0.00	
wu	191.00	53.53	0.00	Stolen *et al.* (1996)
fecf	5.00	13.38	0.00	
fnal	5.00	26.76	0.00	
neph	467.00	10.00	0.80	Holland & Powell (1998)

Notes: 1. Sources of data in addition to those cited in Table A1. 2. Unless otherwise noted, the transition is assumed to be that of magnetic ordering with $T_C = 5$ K, $V_D = 0$ and $S_D = mR\ln(5)$ where m is the number of Fe atoms in the formula unit. 3. Values of V_D and S_D chosen to be vanishingly small.

indicating subtle energetics in the relative stability of these two phases. Indeed, experiments on the $MgAl_2O_4 - NaAlSiO_4$ show wide ranges of coexistence of *cf* and *nal* that we also find in our calculations using our new parameter set (Fig. A5).

We have updated the parameters of several species, including the elasticity and/or equation of state of wadsleyite (Wang *et al.* 2014), diopside (Sang & Bass 2014), hedenbergite (Hu *et al.* 2015), akimotoite (Zhou *et al.* 2014), corundum (Dewaele & Torrent 2013), Na-majorite (Dymshits *et al.* 2013), coesite (Chen *et al.* 2015), stishovite (Wang *et al.* 2012), bridgmanite (Dorfman *et al.* 2013; Zhang *et al.* 2013; Dorfman & Duffy 2014), post-perovskite (Sakai *et al.* 2016), NAL and calcium-ferrite phases (Imada *et al.* 2012; Dai *et al.* 2013; Kojitani *et al.* 2011; Pamato *et al.* 2014; Mookherjee *et al.* 2012) and regular solution parameters of the Calcium-Ferrite (cf) phase to better describe cf-nal phase relations (Ono *et al.* 2009; Imada *et al.* 2011). We have also updated phase equilibria, for example by including experimental data that build on more recent developments in pressure calibration such as the study of the *ri=bg+fp* transition by Ye *et al.* (2017).

The ideal contribution to the chemical potential is completely specified by the chemical formulae of the end-member species (Table A1), as discussed at some length in our previous publication (Stixrude & Lithgow-Bertelloni 2011) and briefly reviewed here. The formulae as written in Table A1 therefore convey not only chemical, but also structural information related to the number of mixing sites, the cations that occupy them, and the nature of the mixing. In order to convey this information, we have found it convenient to adopt the following conventions for writing the chemical formulae. (0) In multisite phases, mixing on sites is independent (uncorrelated). (1) Sites are specified by stoichiometric coefficients: one coefficient for each site (we follow the usual chemical convention of supressing unit coefficients). (2) The number of sites of each end-member of a given phase are the same. (3) The sites appear in the same order in all end-members. (4) Two or more distinct cations that occupy the same crystallographic site in random arrangement are joined by parentheses. (5) Two or more distinct cations that occupy the same site and do not mix are surrounded by square brackets.

APPENDIX C: DERIVATION OF THE RELATIONSHIP BETWEEN THE ISOBARIC AND ISOCHORIC HEAT CAPACITY

The derivation of eq. (24) further illustrates the relationship between isomorphic and metamorphic quantities and makes use of our derivation of the pressure derivative of the species amounts (eq. 22). Expressing the entropy as a function of pressure, temperature, and composition, the differential

$$\mathrm{d}\mathcal{S} = \left(\frac{\partial \mathcal{S}}{\partial P}\right)_{T,\bar{n}} \mathrm{d}P + \left(\frac{\partial \mathcal{S}}{\partial T}\right)_{P,\bar{n}} dT + \sum_i \left(\frac{\partial \mathcal{S}}{\partial n_i}\right)_{P,T,n_{j\neq i}} \mathrm{d}n_i. \tag{C1}$$

Now take the derivative with respect to temperature at constant volume and bulk composition

$$\left(\frac{\partial \mathcal{S}}{\partial T}\right)_{\mathcal{V},\bar{b}} = \left(\frac{\partial \mathcal{S}}{\partial P}\right)_{T,\bar{n}} \left(\frac{\partial P}{\partial T}\right)_{\mathcal{V},\bar{b}} + \left(\frac{\partial \mathcal{S}}{\partial T}\right)_{P,\bar{n}} + \sum_i \left(\frac{\partial \mathcal{S}}{\partial n_i}\right)_{P,T,n_{j\neq i}} \left(\frac{\partial n_i}{\partial T}\right)_{\mathcal{V},\bar{b}}. \tag{C2}$$

Mulitplying by the temperature and using thermodynamic identities

$$C_V = C_{\mathrm{Piso}} - T\mathcal{V}\alpha_{\mathrm{iso}}\alpha K_T + T\sum_i \bar{\mathcal{S}}_i \left(\frac{\partial n_i}{\partial T}\right)_{\mathcal{V},\bar{b}}, \tag{C3}$$

Table A4. Summary of phase equilibria data: stability.

Species	N	P_{min} (GPa)	P_{max} (GPa)	T_{min} (K)	T_{max} (K)	Ref.
fo	4	12.00	13.90	1063	1876	Morishima *et al.* (1994)
mgwa	17	14.88	18.08	1023	1773	Suzuki *et al.* (2000)
		12.10	14.30	1025	1624	Morishima *et al.* (1994)
		21.56	22.46	2173	2173	Fei *et al.* (2004)
mgri	11	14.98	19.50	923	1273	Suzuki *et al.* (2000)
		22.49	24.61	1544	2383	Ye *et al.* (2017)
mgbg+pe	2	22.49	24.61	1544	2383	Ye *et al.* (2017)
en	12	0.00	0.00	823	823	Grover (1972)
		0.00	0.00	1360	1360	Yang & Ghose (1995)
		0.83	0.83	1823	1823	Boyd *et al.* (1964)
		7.70	10.30	1273	1973	Pacalo & Gasparik (1990)
		0.00	10.60	1830	2353	Presnall *et al.* (1998)
mgc2	15	8.20	14.20	1223	1973	Pacalo & Gasparik (1990)
		14.50	15.50	1273	1673	Ito & Navrotsky (1985)
		11.80	14.90	2373	2463	Presnall *et al.* (1998)
mgmj	2	16.50	16.50	2473	2473	Presnall *et al.* (1998)
		21.20	21.20	2273	2273	Hirose *et al.* (2001)
mgil	3	20.00	20.00	1273	1873	Ito & Navrotsky (1985)
		22.13	22.13	1873	1873	Fei *et al.* (2004)
mgbg	16	21.56	24.56	1673	2173	Fei *et al.* (2004)
		21.54	21.54	2273	2273	Hirose *et al.* (2001)
		119.00	149.30	2170	4200	Tateno *et al.* (2009)
		25.00	25.00	2900	2900	Stixrude & Karki (2005)
mgwa+st	5	16.00	18.00	1273	1873	Ito & Navrotsky (1985)
mgri+st	2	19.10	19.10	1373	1673	Ito & Navrotsky (1985)
fs	8	5.00	7.00	1173	1578	Woodland & Angel (1997)
		1.35	1.53	1173	1323	Bohlen *et al.* (1980)
fec2	10	5.50	7.50	1173	1568	Woodland & Angel (1997)
		8.30	9.40	1063	1483	Akimoto & Syono (1970)
feri+st	3	9.40	9.80	1063	1423	Akimoto & Syono (1970)
wu+st	4	17.40	19.80	1473	1873	Katsura *et al.* (1998)
fa	5	4.18	5.56	1073	1473	Yagi *et al.* (1987)
feri	18	4.32	6.28	773	1473	Yagi *et al.* (1987)
		14.80	17.20	1273	1673	Katsura *et al.* (1998)
di	8	0.00	0.00	1665	1665	Boyd & England (1963)
		14.00	14.00	2400	2400	Gasparik (1996a)
		16.50	17.50	1273	2073	Akaogi *et al.* (2004)
capv+mgwa+st	4	17.50	19.00	1273	1673	Akaogi *et al.* (2004)
capv+mgri+st	4	19.00	20.50	1473	1673	Akaogi *et al.* (2004)
capv+mgil	6	20.50	22.50	1473	2073	Akaogi *et al.* (2004)
capv+mgbg	3	22.30	23.00	1873	2073	Akaogi *et al.* (2004)
capv+co	2	24.27	26.16	1673	1873	Takafuji *et al.* (2002)
st	27	101.00	127.00	800	3000	Murakami *et al.* (2003)
		7.71	11.36	800	1803	Zhang *et al.* (1996)
apbo	4	124.00	151.00	2040	2420	Murakami *et al.* (2003)
mppv	8	136.10	171.00	1640	4380	Tateno *et al.* (2009)
pe+co	4	20.00	27.00	1473	1873	Akaogi *et al.* (1999)
		45.00	45.00	1	1	Ono *et al.* (2008)
mgcf	4	27.00	27.00	1873	2173	Akaogi *et al.* (1999)
		45.00	45.00	1	1	Ono *et al.* (2008)
jd+st	3	22.00	22.00	1073	1473	Yagi *et al.* (1994)
nacf+st	2	23.00	23.00	1273	1473	Yagi *et al.* (1994)
ab	12	1.60	3.30	873	1473	Holland (1980)
jd+qtz	1	1.65	1.65	873	873	Holland (1980)
coes	16	7.91	8.62	1258	1507	Zhang *et al.* (1996)
		2.48	2.98	673	1273	Bohlen & Boettcher (1982)
qtz	11	2.46	2.95	673	1273	Bohlen & Boettcher (1982)
cats	3	1.72	2.85	1573	1773	Gasparik (1984)
gr+co	3	1.77	2.88	1573	1773	Gasparik (1984)
fa+qtz	4	1.10	1.40	1073	1273	Bohlen *et al.* (1980)
ky	4	0.75	0.82	1073	1073	Harlov & Milke (2002)
qtz+co	2	0.70	0.75	1073	1073	Harlov & Milke (2002)
gr+ky+qtz	24	2.20	3.10	1373	1673	Goldsmith (1980)
an	1	3.00	3.00	1673	1673	Goldsmith (1980)

Table A4. Continued

Species	N	P_{min} (GPa)	P_{max} (GPa)	T_{min} (K)	T_{max} (K)	Ref.
jd	1	2.38	2.38	1473	1473	Gasparik (1985)
neph+ab	1	2.33	2.33	1473	1473	Gasparik (1985)
jd+anao	6	16.00	19.00	1273	1873	Akaogi et al. (2002)
nacf	6	18.00	27.00	1273	1873	Akaogi et al. (2002)
sp+jd+anao	16	12.00	30.00	1273	1873	Ono et al. (2009)
mnal+nnal	6	14.50	23.00	1273	1873	Ono et al. (2009)
		47.00	47.00	1800	1800	Imada et al. (2011)
mgcf+nacf	1	24.00	24.00	1873	1873	Ono et al. (2009)
co	5	96.90	106.40	1600	3000	Kato et al. (2013)
albg	11	99.90	169.70	1670	3540	Kato et al. (2013)
appv	5	148.90	186.00	2590	3510	Kato et al. (2013)
mgbg+albg	1	137.00	137.00	2000	2000	Tateno et al. (2005)
mppv+appv	1	175.00	175.00	2000	2000	Tateno et al. (2005)
wu+co+st	1	35.00	35.00	2000	2000	Dorfman et al. (2012)
jd+cen	2	13.50	13.50	1823	2373	Gasparik (1992)
py+namj	2	13.50	13.50	1823	2373	Gasparik (1992)

Table A5. Summary of phase equilibrium data: reactions.

Species	N	P_{min} GPa	P_{max} GPa	T_{min} K	T_{max} K	Ref.
py+capv=gr+mgmj	1	19.90	19.90	1873	1873	Saikia et al. (2008)
mgc2=py+mgmj	1	12.50	12.50	1923	1923	Gasparik (1989)
en+di=odi+cen	14	3.00	3.00	1173	1773	Carlson & Lindsley (1988)
he+en=di+fs	1	1.50	1.50	1263	1263	Lindsley (1983)
fo+wu=fa+pe	13	11.00	11.00	1673	1673	Frost (2003b)
fo+al=fa+py	10	0.91	0.91	1273	1273	Hackler & Wood (1989)
mgri+wu=feri+pe	51	11.00	23.50	1273	1873	Frost et al. (2001)
pe+fewa=wu+mgwa	15	13.00	14.50	1673	1673	Frost (2003b)
fo+fewa=fa+mgwa	1	12.87	12.87	1673	1673	Frost (2003b)
mgwa+feri=fewa+mgri	1	12.87	12.87	1673	1673	Frost (2003b)
mgbg+wu=febg+pe	2	25.00	25.00	2000	2541	Nakajima et al. (2012)
mgil+febg=feil+mgbg	2	25.50	25.50	1373	1373	Ito & Yamada (1982)
		24.00	24.00	2073	2073	Ohtani et al. (1991)
fo+hc=fa+sp	13	0.00	0.00	1573	1573	Jamieson & Roeder (1984)
mgts+en=co+py	1	1.65	1.65	1123	1123	Gasparik & Newton (1984)
mgts=en+py	23	2.07	4.01	1173	1773	Perkins et al. (1981)
en+sp=mgts+fo	6	0.99	2.56	1573	1773	Gasparik & Newton (1984)
mgts+di+cen=cats+en+odi	6	2.70	2.70	1773	1773	Klemme & O'Neill (2000)
		2.50	2.50	1173	1173	Perkins & Newton (1980)
gr+py+cen=di+cats	1	2.50	2.50	1173	1173	Perkins & Newton (1980)
gr+py=co+di+cats+cen	1	3.25	3.25	1573	1573	Gasparik (1984)
jd+di=qtz+ab	21	0.85	1.60	873	873	Holland (1983)
mgc2=cen+jd	1	13.50	13.50	1923	1923	Gasparik (1992)
mgc2+mgmj=namj+py	1	14.00	14.00	1923	1923	Gasparik (1992)
mnal+nacf=nnal+mgcf	1	23.00	23.00	1873	1873	Ono et al. (2009)
mnal+nnal=nacf+mgcf	1	23.00	23.00	1873	1873	Ono et al. (2009)
mnal=mgcf+nacf	1	25.00	25.00	1873	1873	Ono et al. (2009)
fnal+mgcf=mnal+fecf	2	23.00	23.00	1673	2073	This Work (2014)
febg+mgcf=mgbg+fecf	2	60.00	60.00	2000	2400	Hirose et al. (2005)
mgil+co=mgbg+albg	2	27.00	27.00	2300	2300	Liu et al. (2017)
febg+mgbg=wu+pe+st	2	22.00	22.00	2273	2273	Tange et al. (2009)

where we have also used the definition of the partial molar entropy. We can express the temperature derivative of the species amounts

$$\left(\frac{\partial n_i}{\partial T}\right)_{\mathcal{V},\vec{b}} = \left(\frac{\partial n_i}{\partial T}\right)_{P,\vec{b}} + \left(\frac{\partial n_i}{\partial P}\right)_{T,\vec{b}} \left(\frac{\partial P}{\partial T}\right)_{\mathcal{V},\vec{b}} \tag{C4}$$

which we substitute into eq. (C3) yielding

$$C_V = C_P - T\mathcal{V}\alpha K_T \alpha_{iso} + T\alpha K_T \sum_i \bar{\mathcal{S}}_i \left(\frac{\partial n_i}{\partial P}\right)_{T,\vec{b}} \tag{C5}$$
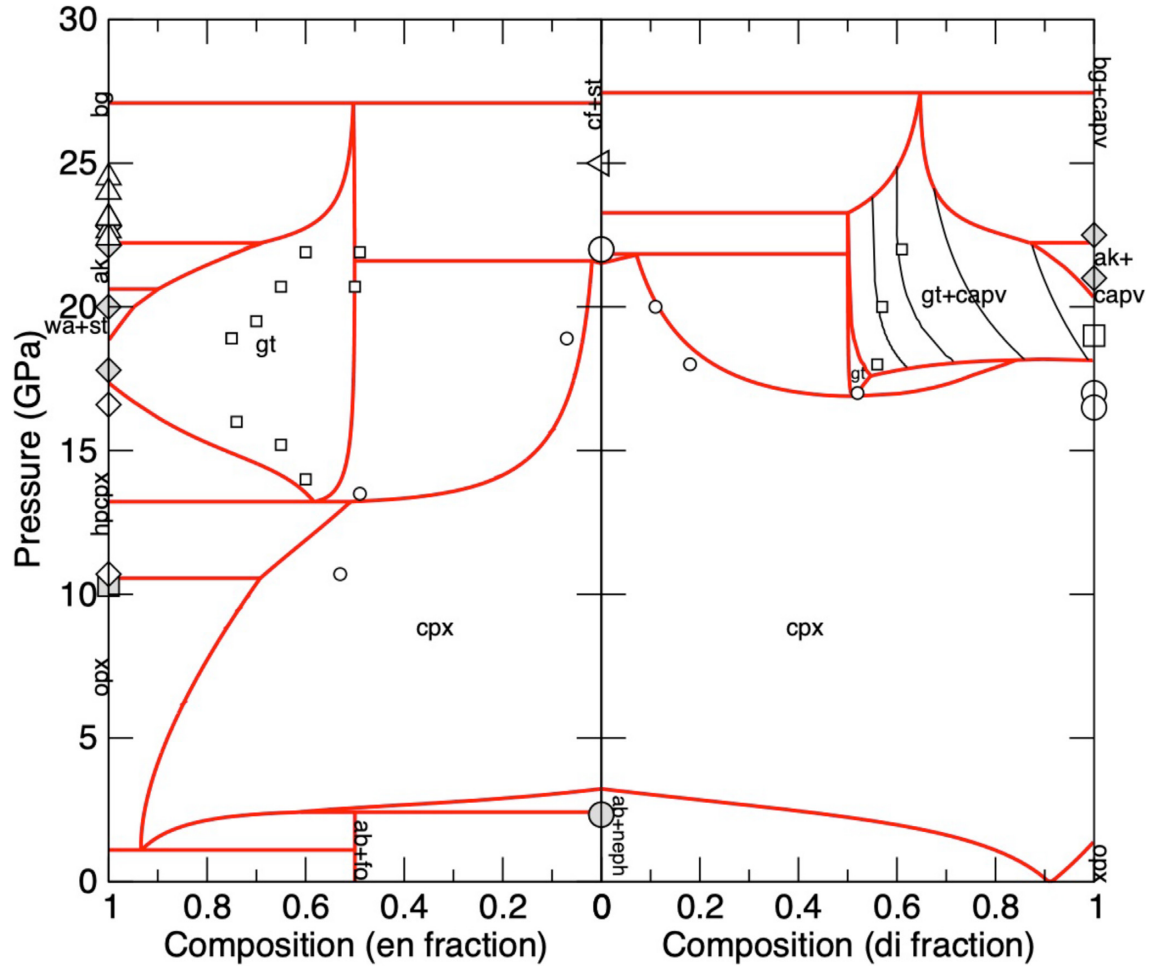
Figure A3. Phase equilibria computed with HeFESTo at 1923 K (red lines) compared with experimental observations of stability (large symbols) or phase compositions (small symbols). (Left) the enstatite-jadeite join with composition plotted as mole fraction (MgMg/(NaAl+MgMg)). (right) the jadeite-diopside join with composition plotted as mole fraction (CaMg/(CaMg+NaAl)). Also shown in the right hand figure are contours of the atomic fraction of *capv* within the *capv* + *gt* stability field, from left to right: 10 per cent, 20 per cent, 30 per cent, 40 per cent. Experimental data: *cpx* (open circles) (Canil 1994; Akaogi *et al.* 2004; Gasparik 1996b, 1992); *ab* + *neph* (filled circles) (Gasparik 1985); *opx* (filled squares) (Pacalo & Gasparik 1990); *hpcpx* (open diamond) (Pacalo & Gasparik 1990); *gt* (open square) (Gasparik 1992; Akaogi *et al.* 2004; Gasparik 1996b); *ak* and *ak* + *capv* (filled diamond) (Ito & Takahashi 1989; Gasparik 1990; Ito & Navrotsky 1985; Fei *et al.* 2004; Akaogi *et al.* 2004); *bg* (open triangle) (Ito & Takahashi 1989; Fei *et al.* 2004); *cf* + *st* (left-pointing open triangle) (Liu 2006).

and we have also used eq. (9). Now, we substitute our result for the pressure derivative of the species amounts (eq. 22)

$$C_V = C_P - T\mathcal{V}\alpha K_T\alpha_{\mathrm{iso}} - T\alpha K_T \sum_{ij} \bar{\mathcal{S}}_i M_{ij} \bar{\mathcal{V}}_j. \tag{C6}$$

According to eq. (20), the sum is just $\mathcal{V}\alpha_{\mathrm{met}}$ (M_{ij} is symmetric), so combining terms

$$C_V = C_P - T\mathcal{V}\alpha K_T\alpha \tag{C7}$$

Finally, we combine this equation with the definition of the Grüneisen parameter

$$\gamma = \frac{\mathcal{V}\alpha K_T}{C_P} \tag{C8}$$

to obtain eq. (24). The derivation of the relationship between adiabatic and isothermal bulk moduli (eq. 25) is similar. The equation for the Grüneisen parameter (eq. 26) follows from eqs (24) and (25) and the definition of γ.
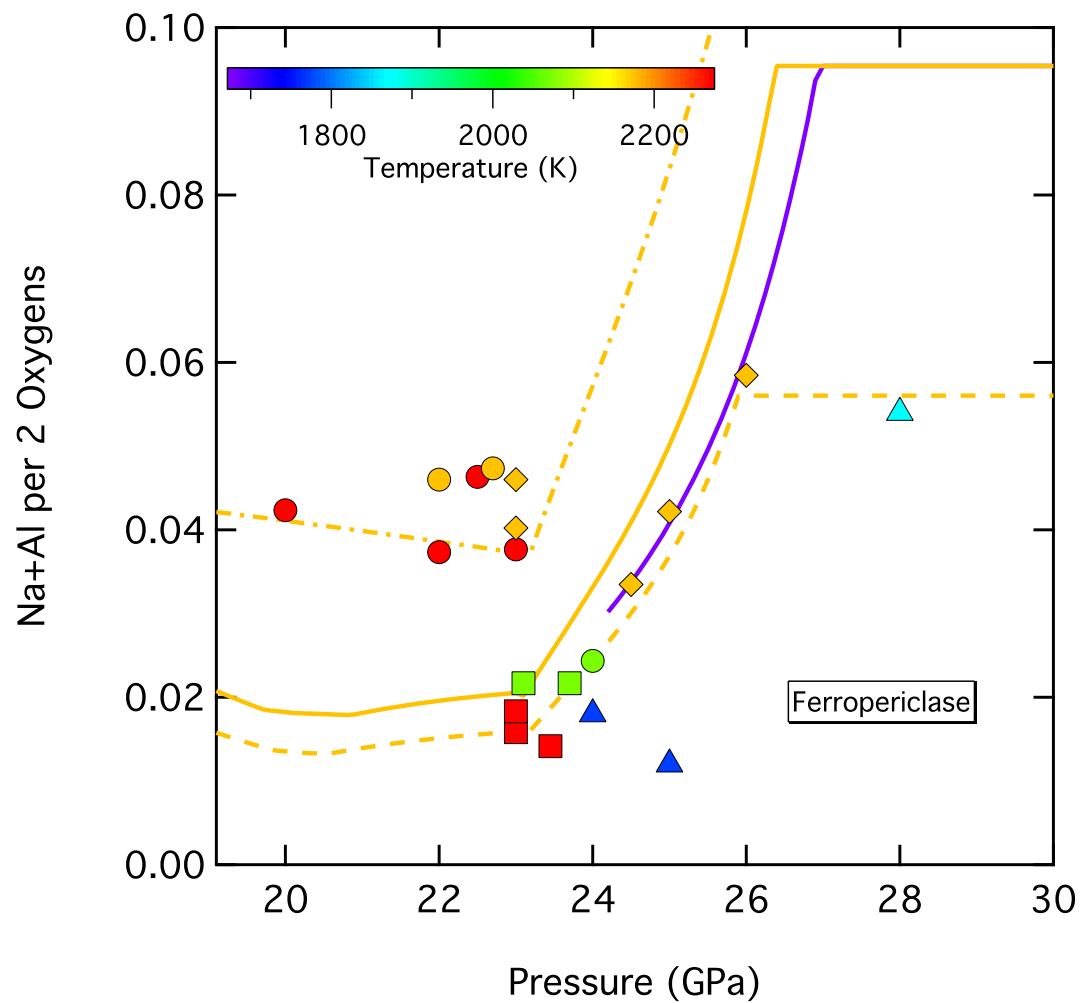
Figure A4. Na+Al content of the ferropericlase phase computed with HeFESTo: solid lines (KLB-1 bulk composition), dashed line (Tinaquillo lherzolite), dash–dotted line (chondritic composition of (Gasparik 2000)) compared with experimental measurements: triangles (Irifune 1994), squares (Hirose 2002), diamonds (Wood 2000) and circles (Gasparik 2000). All lines and symbols are colour-coded according to the temperature scale shown.
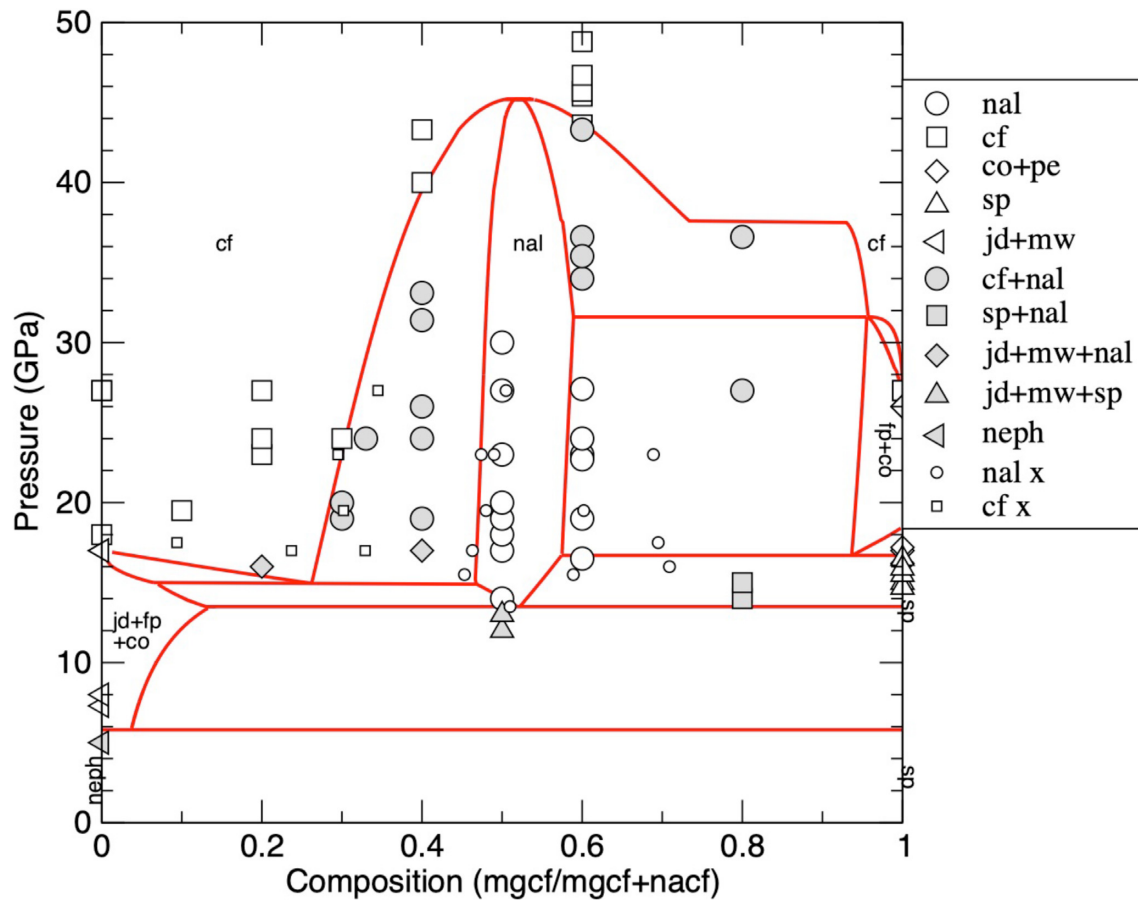
Figure A5. Phase equilibria on the join $MgAl_2O_4 - NaAlSiO_4$ as computed with HeFESTo at 1873 K (red lines) and according to experimental measurements with large symbols indicating observations of stability and small symbols indicating measurements of phase compositions according to the legend. Sources of data are: *nal* stability (Ono *et al.* 2009), *cf* stability (Ono *et al.* 2009; Akaogi *et al.* 2002, 1999; Imada *et al.* 2011), *co+pe* stability (Ono *et al.* 2009; Akaogi *et al.* 1999), *sp* stability (Ono *et al.* 2009; Akaogi *et al.* 1999), *jd+sp* stability (Ono *et al.* 2009; Akaogi *et al.* 2002), *cf+nal* stability (Ono *et al.* 2009; Imada *et al.* 2011), *sp+nal* stability (Ono *et al.* 2009), *jd+fp+nal* stability (Ono *et al.* 2009), *jd+fp+sp* stability (Ono *et al.* 2009), *neph* stability (Akaogi *et al.* 2002), *cf* and *nal* compositions (Ono *et al.* 2009).